


## Mg-based compounds for hydrogen and energy storage

J.-C. Crivello<sup>1</sup> · R. V. Denys<sup>2</sup> · M. Dornheim<sup>3</sup> · M. Felderhoff<sup>4</sup> · D. M. Grant<sup>5</sup> ·  
J. Huot<sup>6</sup> · T. R. Jensen<sup>7</sup> · P. de Jongh<sup>8</sup> · M. Latroche<sup>1</sup> · G. S. Walker<sup>5</sup> ·  
C. J. Webb<sup>9</sup> · V. A. Yartys<sup>2</sup> 

Received: 29 September 2015 / Accepted: 3 January 2016 / Published online: 22 January 2016  
© Springer-Verlag Berlin Heidelberg 2016

**Abstract** Magnesium-based alloys attract significant interest as cost-efficient hydrogen storage materials allowing the combination of high gravimetric storage capacity of hydrogen with fast rates of hydrogen uptake and release and pronounced destabilization of the metal–hydrogen bonding in comparison with binary Mg–H systems. In this review, various groups of magnesium compounds are considered, including (1) RE–Mg–Ni hydrides (RE = La, Pr, Nd); (2) Mg alloys with *p*-elements (X = Si, Ge, Sn, and Al); and (3) magnesium alloys with

*d*-elements (Ti, Fe, Co, Ni, Cu, Zn, Pd). The hydrogenation–disproportionation–desorption–recombination process in the Mg-based alloys (LaMg<sub>12</sub>, LaMg<sub>11</sub>Ni) and unusually high-pressure hydrides synthesized at pressures exceeding 100 MPa (MgNi<sub>2</sub>H<sub>3</sub>) and stabilized by Ni–H bonding are also discussed. The paper reviews interrelations between the properties of the Mg-based hydrides and *p*–*T* conditions of the metal–hydrogen interactions, chemical composition of the initial alloys, their crystal structures, and microstructural state.

✉ C. J. Webb  
j.webb@griffith.edu.au

✉ V. A. Yartys  
volodymyr.yartys@ife.no; volodymyr.yartys@gmail.com

J.-C. Crivello  
crivello@icmpe.cnrs.fr

R. V. Denys  
roman.v.denys@gmail.com

M. Dornheim  
martin.dornheim@hzg.de

M. Felderhoff  
felderhoff@mpi-muelheim.mpg.de

D. M. Grant  
David.Grant@nottingham.ac.uk

J. Huot  
jacques.huot@uqtr.ca

T. R. Jensen  
trj@chem.au.dk

P. de Jongh  
P.E.deJongh@uu.nl

M. Latroche  
latroche@icmpe.cnrs.fr

G. S. Walker  
Gavin.Walker@nottingham.ac.uk

- <sup>1</sup> Université Paris Est, ICMPE (UMR 7182), CNRS, UPEC, 2 rue Henri Dunant, Thiais F-94320, France
- <sup>2</sup> Institute for Energy Technology and Norwegian University of Science and Technology, Kjeller and Trondheim, Norway
- <sup>3</sup> Helmholtz-Zentrum Geesthacht, Zentrum für Material- und Küstenforschung GmbH, Geesthacht, Germany
- <sup>4</sup> Max-Planck-Institut für Kohlenforschung, Kaiser-Wilhelm-Platz 1, 45470 Mülheim an der Ruhr, Germany
- <sup>5</sup> Nottingham University, Nottingham, UK
- <sup>6</sup> Hydrogen Research Institute, Université du Québec à Trois-Rivières, 3351 Boulevard des Forges, Trois-Rivières, QC, Canada
- <sup>7</sup> Department of Chemistry, Interdisciplinary Nanoscience Center, Aarhus University, Langelandsgade 140, 8000 Aarhus C, Denmark
- <sup>8</sup> Debye Institute for Nanomaterials Science, Utrecht University, Utrecht, Netherlands
- <sup>9</sup> Queensland Micro- and Nanotechnology Centre, Griffith University, Brisbane, Australia

## 1 Introduction

This work is a review of the recent progress made in the past years, particularly in the framework of the International Energy Agency Task 32 Hydrogen-based Energy Storage, in the area of fundamental and applied studies of Mg-based compounds for hydrogen and energy storage.

In order to find a hydrogen storage system that meets the requirements of low weight (for mobile applications) and adequate capacity, chemical hydrides based on lightweight metals have been extensively investigated [1, 2]. Due to the low cost of extraction from natural chlorides and carbonates which form a significant part of the earth's crust and oceans, magnesium, a lightweight alkaline earth metal, fits many of these requirements.

The reaction of magnesium with hydrogen yields magnesium dihydride ( $\text{MgH}_2$ ) and is reversible, with a storage capacity of 7.6 wt% of hydrogen. The hydrogenation process, however, suffers from slow kinetics, and the dehydrogenation of  $\text{MgH}_2$  requires temperatures exceeding 300 °C, which is impracticable for mobile applications and constitutes a significant net energy loss for any system based on  $\text{MgH}_2$ .

The kinetics have been shown to improve by crystallite size reduction which allows for shorter hydrogen diffusion paths and the introduction of defects in the material which provides faster pathways for hydrogen to diffuse [3–5]. The introduction of small amounts of additives (typically transition metals and transition metal oxides, but also carbons [6, 7]) has also improved the kinetic rates of absorption and desorption significantly [8]. However, reducing the equilibrium temperature of desorption relies on lowering the thermodynamic enthalpy, and one of the more promising pathways for this is the formation of magnesium alloys with other metals.

Materials suitable for the storage of hydrogen and heat can play an important role for future climate policy goals, because they can compensate for fluctuations in the production of electricity from the renewable energy sources. Of particular interest are metal hydride compounds because these compounds connect energy production and storage with a future hydrogen economy.

Mg-based metal hydrides can be used as solid-state hydrogen storage materials for fuel cell cars, as a hydrogen source for fuel cell auxiliary power units, for the storage of high-temperature heat in industrial processes and in power plants, or for the smoothing of irregular supply of heat and electricity production for fuel cells in domestic energy sectors.

Metal hydrides are produced from different pure metals or metal alloys under the influence of hydrogen. This process of hydrogenation is accompanied by the release of heat (exothermic reaction). The same amount of heat must be supplied to the metal hydride for the decomposition and the release of hydrogen (endothermic reaction, see Eq. 1). These processes are infinitely repeatable, and reversible Mg-based metal hydrides can therefore be used for the storage of heat and hydrogen [9]. Depending on the thermodynamics of the reaction, different temperatures apply to different metal hydrides (Table 1).



### 1.1 Thermodynamic tuning

The temperature required to generate 1 bar of hydrogen from a hydride system can be calculated from the change in enthalpy and entropy for dehydrogenation, as shown in Eq. 2. Thermodynamic tuning of a multicomponent hydride system requires the addition of a second phase (Z) to the hydride ( $\text{YH}_2$ ), which reacts with the hydride, releasing hydrogen and generating a new alloy or compound (YZ) [12]. As can be seen from Fig. 1, the reduction in the enthalpy for dehydrogenation is determined by the enthalpy of formation for the alloy or compound formed, as shown in Eq. 3.

$$T(1 \text{ bar}) = \Delta H / \Delta S \quad (2)$$

$$\Delta H_b = \Delta H_a + \Delta H_f \quad (3)$$

### 1.2 Mg alloys with *p*-elements (X = Al, Si, Ge, Sn)

#### 1.2.1 Silicon

Silicon has a very low solubility in magnesium of 0.003 %. When  $\text{MgH}_2$  mixed with Si is heated until the hydrogen is

**Table 1** Selected physical data of Mg-based metal hydrides for hydrogen and heat storage applications

Material	H content (wt%)	$\Delta H_r$ (kJ/mol $\text{H}_2$ )	Heat storage density (kWh/kg)	Equilibrium temperature at 0.1 MPa (°C)	References
$\text{MgH}_2$	7.7	74	0.78	280	[10]
$\text{NaMgH}_3$	4.0	86.6	0.47	380	[11]
$\text{Mg}_2\text{NiH}_4$	3.6	62	0.31	250	[10]
$\text{Mg}_2\text{FeH}_6$	5.5	77	0.55	320	[10]

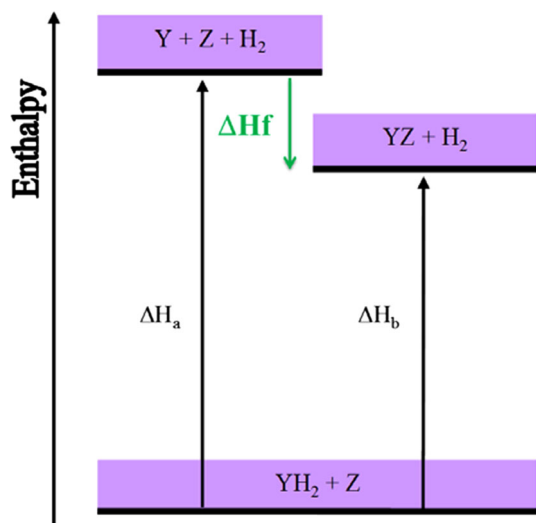


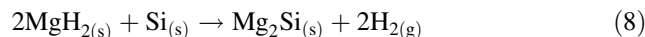
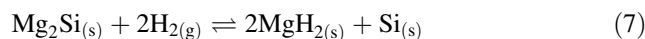
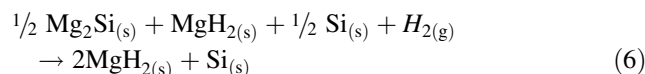
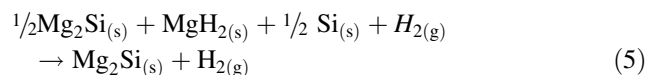
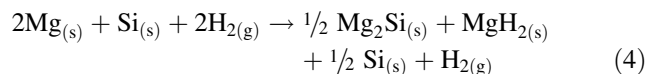
**Fig. 1** Thermodynamic tuning for multicomponent systems

released, it forms the intermetallic  $\text{Mg}_2\text{Si}$  [13]. While the reaction is reversible in a ball-mill environment with hydrogen [14–16], application of pressures of hydrogen to  $\text{Mg}_2\text{Si}$  up to 185 MPa and 350 °C has not yielded a hydride phase [13, 17] except when the  $\text{Mg}_2\text{Si}$  particle size was reduced to 10 nm. Even then, the yield was low and the kinetics very poor [18].

Bystrzycki et al. [19] observed only the metastable  $\text{Mg}_5\text{Si}_6$  in a study of the destabilization of  $\text{MgH}_2$  by Si, where Si was deposited by pulsed laser deposition on a  $\text{MgH}_2/\text{Mg}$  substrate and did not find any destabilization.

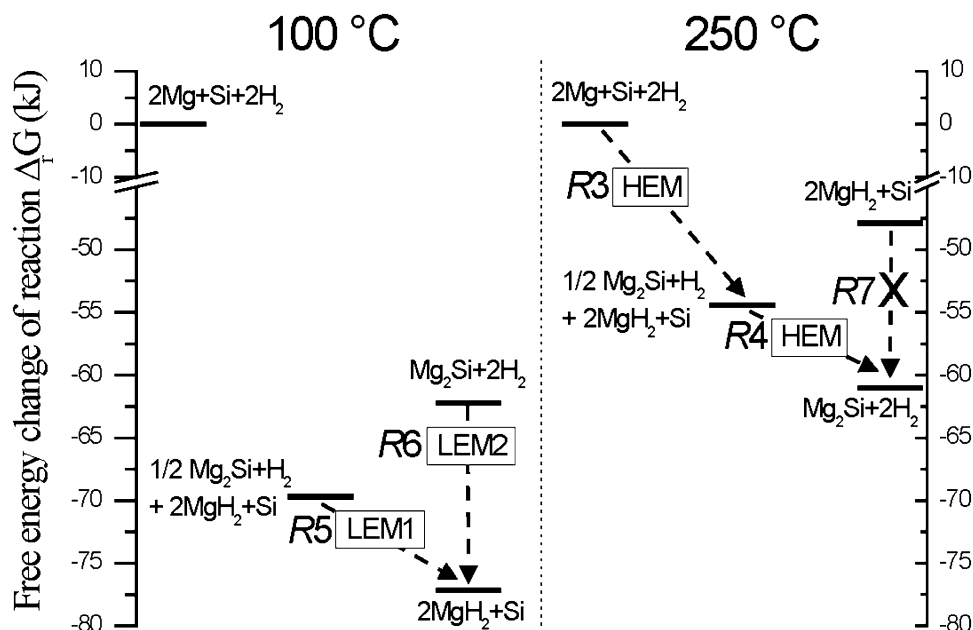
However, the Mg–Si–H system has been studied with regard to its hydrogen storage properties. Samples were

prepared by reactive ball-milling under hydrogen, and depending on the milling conditions, different paths can be obtained. For high rotation speeds,  $\text{Mg}_2\text{Si}$  is formed, whereas  $2\text{MgH}_2 + \text{Si}$  are obtained at low rotation speeds. This behaviour can be understood by considering the change in local temperature at the collision impact with milling speed. On this basis, it is observed that the reaction  $\text{Mg}_2\text{Si} + 2\text{H}_2 \rightleftharpoons 2\text{MgH}_2 + \text{Si}$  is reversible. The hydrogenation reaction can be achieved by milling  $\text{Mg}_2\text{Si}$  at low rotation speed, whereas the reverse reaction can be triggered by milling at high rotation speed. However, a small quantity of  $\text{Mg}_2\text{Si}$  is necessary to initiate the reaction between magnesium hydride and silicon.



As shown in Fig. 2, starting from the elements, after 4 h of high-energy milling (HEM) under hydrogen, a metastable state is reached where three solid phases coexist ( $\text{MgH}_2$ , Si, and  $\text{Mg}_2\text{Si}$ ). At this stage, further milling keeping to the HEM regime leads to the formation of  $\text{Mg}_2\text{Si}$  without  $\text{H}_2$  absorption, whereas low-energy milling (LEM) allows the formation of  $\text{MgH}_2 + \text{Si}$  with full

**Fig. 2** Free energy diagrams, showing milling reagents and obtained products for two pressure–temperature conditions (100 and 250 °C at  $p(\text{H}_2) = 9 \text{ MPa}$ )



hydrogen absorption. It is therefore possible to tune the reaction by switching from HEM to LEM. The final products are dependent on the milling energy which probably governs the local temperature at milling impact (Eqs. 4–8). Interestingly, the full conversion of  $\text{Mg}_2\text{Si} + \text{H}_2$  into  $\text{MgH}_2 + \text{Si}$  is also possible by LEM. However, the reverse reaction could not be obtained by HEM probably due to kinetic limitations at the  $\text{MgH}_2/\text{Si}$  interfaces. Such limitations are overcome by the presence of  $\text{Mg}_2\text{Si}$  in three-phase mixtures. Contrary to solid/gas reactions, the present work shows that reversible hydrogen storage in  $\text{Mg}_2\text{Si}$  can be achieved by ball-milling at room temperature under moderate hydrogen pressure (9 MPa).

The free-energy change,  $\Delta_r G_p^T$ , of the reactions observed in this study is displayed in Fig. 2. By increasing the local temperature, the energy level of  $\text{MgH}_2$  increases as compared to  $\text{Mg}_2\text{Si}$ . Indeed, the large entropy change associated with the absorption of molecular hydrogen from the gas phase into atomic hydrogen in the Mg lattice accounts for the high variation in  $\Delta_r G_p^T$  with temperature. As a consequence, while at low temperatures (e.g. 100 °C)  $\Delta_r G_p^T$  is lower for  $\text{MgH}_2$  than for  $\text{Mg}_2\text{Si}$ , the opposite occurs at high temperatures (e.g. 250 °C). At the imposed pressure conditions ( $\sim 9$  MPa), the crossover temperature is 180 °C. Thus, we argue that under LEM conditions, the reaction temperatures are below 180 °C leading to  $\text{MgH}_2 + \text{Si}$  as stable phases. In contrast, local temperatures above 180 °C occur under HEM conditions, and  $\text{Mg}_2\text{Si}$  is produced.

### 1.2.2 Germanium

Germanium can also be used to reduce the enthalpy of dehydrogenation from  $\text{MgH}_2$ , through the formation of magnesium germanide,  $\text{Mg}_2\text{Ge}$  (see Fig. 3) [16]. The enthalpy of formation for  $\text{Mg}_2\text{Ge}$  is 104.6 kJ/mol, which gives an enthalpy of dehydrogenation for  $2\text{MgH}_2:\text{Ge}$  of

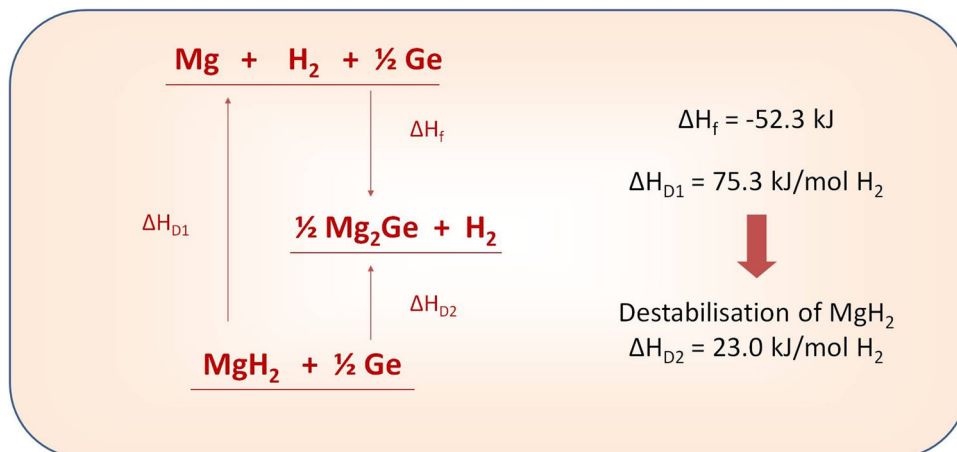
23.0 kJ/mol, yielding a  $T(1 \text{ bar})$  of  $-91.6$  °C [20]. Interest in the use of Ge was initially as an additive for improving the kinetics of  $\text{MgH}_2$  [21]. Ball-milling the elements Mg and Ge together led to the formation of  $\text{Mg}_2\text{Ge}$  dispersed in a Mg matrix. Unfortunately, the  $\text{Mg}_2\text{Ge}$  was not found to have any positive effect on the hydrogenation of the remaining Mg. Ball-milling  $\text{MgH}_2$  with Ge was found to be an effective way to limit the formation of  $\text{Mg}_2\text{Ge}$  phase, but still produces an intimate mixture of the two starting phases [20]. It has also been found that ball-milling  $\text{MgH}_2$  and Ge under a hydrogen atmosphere reduces the amount of  $\text{Mg}_2\text{Ge}$  formed even further, presumably through suppressing the formation of Mg metal during milling, which reacts more readily with the Ge [22].

High-pressure DSC results gave a dehydrogenation endothermic peak at 235 °C (regardless of the hydrogen back pressure used, from 0 to 25 bar) [20]. Modifying the sample with a Ti-based additive reduced the dehydrogenation even further, starting at 130 °C (also confirmed in Fig. 4). The kinetics of the reaction were investigated, the unmodified system released hydrogen very quickly at 250 °C, taking only 15 min. Dehydrogenation was more sluggish at 200 °C, only reaching 60 % conversion after 60 min (Fig. 4). However, adding a Ti-based additive gave fast kinetics at 200 °C, with complete conversion within 15 min. These are very favourable results in comparison with the silicide analogues where, after 5 h at 250 °C, the reaction was still not complete for Ti-modified  $2\text{Mg}:\text{Si}$  [23].

### 1.2.3 Tin

$\text{Mg}_2\text{Sn}$  can be prepared either by powder metallurgy or by ball-milling under an argon atmosphere [16]. Powder metallurgy leads to a cubic antiferroite structure as for Ni and Ge, whereas with ball-milling, a metastable rhombohedral phase is obtained. Such a metastable phase is also

**Fig. 3** Destabilization of  $\text{MgH}_2$  with Ge [19]



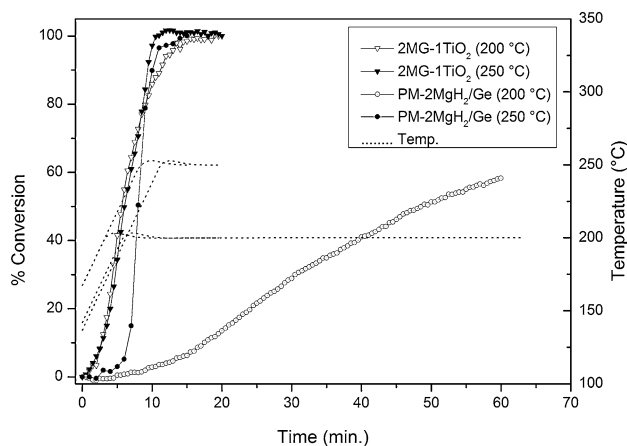


**Fig. 4** TGA data for the dehydrogenation of  $2\text{MgH}_2/\text{Ge}$  samples with and without a Ti-based additive. Samples were ball-milled for 140 min; TGA used a flowing Ar carrier

observed at high pressure (60 kbar, 900 °C) and is possibly stabilized by a magnesium deficiency leading to the  $\text{Mg}_9\text{Sn}_5$  stoichiometry instead of the 2:1 ratio. The cubic phase obtained by powder metallurgy was ball-milled under hydrogen gas (20 bar). No hydrogen uptake could be observed, but the formation of the rhombohedral phase occurred in a shorter time (3 h) than milling under argon (12 h). The decomposition of  $\text{Mg}_2\text{Sn}$  was not observed, even for long milling times, but the rapid formation of the rhombohedral phase under hydrogen can be understood by the formation of small quantities of  $\text{MgH}_2$  leading to the Mg-deficient  $\text{Mg}_9\text{Sn}_5$  rhombohedral compound [14].

#### 1.2.4 Aluminium

A sample of  $\gamma\text{-Mg}_{17}\text{Al}_{12}$ , produced by arc-melting and BM, transformed completely to  $\text{MgH}_2$  and metallic Al during hydrogenation ( $p(\text{H}_2) = 30$  bar,  $T = 350$  °C,  $t = 17$  h) [24]. The apparent activation energy for decomposition of air-exposed  $\text{MgH}_2\text{-Al}$  is estimated as  $E_A \sim 160$  kJ/mol  $\text{H}_2$  [24]. This value corresponds to the activation barrier of 160–166 kJ/mol  $\text{H}_2$  for the dehydrogenation of pure magnesium hydride [25, 26]. The alloying with Al creates an alloy which is less sensitive towards oxygen contamination and which requires little if any pre-treatment in order to activate [24].

### 1.3 Magnesium alloys with *d*-elements (Ni, Cu, Co, Ti, Pd, Fe, Zn)

#### 1.3.1 Nickel

The addition of Ni to the Mg system can be beneficial for different reasons. Nickel is a very good (de)hydrogenation catalyst, which means that it facilitates the absorption and

desorption of hydrogen by adsorbing and dissociating hydrogen molecules into adsorbed atomic species and vice versa. It is not necessary to have pure Ni in the system, and Mg–Ni alloys also show these enhanced sorption kinetics [26–28]. For instance, enhanced hydrogen sorption rates, while retaining a high storage capacity of about 6 wt% hydrogen, were obtained for  $\text{Mg}_{1-x}\text{Ni}_x$  alloys with different compositions ( $0 \leq x \leq 0.33$ ) prepared by melt spinning [27]. A second aspect is that in the processing of Mg materials, such as ball-milling or nanoconfinement, Ni often has an influence on the structural properties of the resulting material [29].

However, the most important aspect is the possibility to form alloys. The thermodynamic properties for hydrogen desorption from  $\text{Mg}_2\text{NiH}_4$  are considerably more favourable than those of  $\text{MgH}_2$ , with a formation enthalpy for  $\text{Mg}_2\text{NiH}_4$  of about  $-64$  kJ/mol (decreasing the equilibrium hydrogen desorption temperature under 1 bar  $\text{H}_2$  from 300 to 250 °C). Unfortunately, the addition of nickel also significantly reduces the capacity, with  $\text{Mg}_2\text{NiH}_4$  only containing 3.6 wt% of hydrogen [30].

Recent developments are mostly related to further insight into the properties of  $\text{Mg}_x\text{Ni}$  alloys by studying the hydrogenation properties of thin films [31, 32] and nanoparticles, prepared either by supporting on a carbon scaffold [33] or by gas-phase techniques [22, 23]. Using an in situ microscope during hydrogenation, it was possible to visualize the nucleation and growth of  $\text{Mg}_2\text{NiH}_4$  crystals with a lattice spacing of 0.22 nm in Mg-rich domains, followed by crystallization of  $\text{MgH}_2$ , demonstrating how the presence of  $\text{Mg}_2\text{Ni}$  facilitates the hydrogenation of Mg [32]. In addition, measurements on nanoparticles produced by inert gas condensation clearly connected the enhancement of the hydrogen sorption properties to the formation of  $\text{Mg}_2\text{Ni}$  and  $\text{Mg}_2\text{NiH}_4$  phases [23].  $\text{Mg}_2\text{Ni}$ , particularly in a form prepared by rapid solidification nanocomposite with Mg [34], enhances the hydrogenation of the Mg-based alloys allowing higher rates of hydrogen absorption and desorption.

Since Ni destabilizes the magnesium–hydrogen bonding, this results in the reduction in the decomposition temperatures of the formed hydrides, as demonstrated for Mg–Mm–Ni alloy-based hydrides nanostructured by Equal Channel Angular Pressing in [35]. The effect of nickel is associated with strong covalent Ni–H bonding which leads to the formation of various types of Ni–H complexes and clusters,  $[\text{NiH}_4]^{4-}$  tetrahedra in the case of  $\text{Mg}_2\text{NiH}_4$  or buckled nets  $-\text{Ni}-\text{H}-\text{Ni}-\text{H}-$  penetrating through the structure in the recently studied  $\text{MgNi}_2\text{H}_3$  [36]. While in both cases the metal sublattice requires a complete rebuilding, for the Laves-type intermetallic  $\text{MgNi}_2$ , a hydrogen-induced transformation takes place in the metal sublattice when a very high hydrogen pressure of 28 kbar



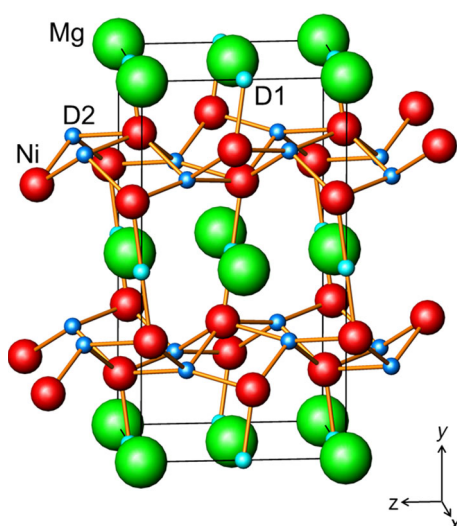


**Fig. 5** Crystal structure of  $\text{MgNi}_2\text{D}_3$ . Two types of sites occupied by deuterium include a  $\text{Mg}_4\text{Ni}_2$  octahedron for H1(D1) and a chair  $\text{Ni}_4$  configuration for H2(D2) located within the buckled Ni–H nets containing bent spirals  $-\text{Ni}-\text{H}_2-\text{Ni}-\text{H}_2-$

$\text{H}_2$  is applied at a temperature of 300 °C. Surprisingly, instead of a disproportionation to form  $\text{MgH}_2$ , the hydrogenation leads to a rebuilding of the initial hexagonal structure into the orthorhombic distorted  $\text{MoSi}_2$ -type sublattice. In the formed  $\text{MgNi}_2\text{H}_3$ , H atoms fill the deformed octahedra  $\text{Mg}_4\text{Ni}_2$  and the positions within the buckled nets  $-\text{Ni}-\text{H}-\text{Ni}-\text{H}-$  penetrating through the structure (Fig. 5). Analysis of the electronic structure revealed a charge transfer from Mg to Ni, and to the H atoms. The calculated gross heat of formation for the *Cmca* phase of  $\text{MgNi}_2\text{H}_3$  is  $\sim 37.3$  kJ/mol- $\text{H}_2$ , which is consistent with the stability of the hydride at normal conditions.

### 1.3.2 Copper

No ternary hydrides have been reported in the literature for the Mg–Cu system. However, the role of copper is to substitute the hydrogen in the  $\text{MgH}_2$  and form a stable compound,  $\text{Mg}_2\text{Cu}$ .  $\text{Mg}_2\text{Cu}$  disproportionates during hydrogenation as described in Eq. 9.



Thus, the alloy  $\text{Mg}_2\text{Cu}$  has a theoretical hydrogen capacity of  $\rho_m = 2.62$  wt% H, and  $\Delta H_f = -70$  kJ/mol  $\text{H}_2$  [37, 38].

A sample of Mg/ $\text{Mg}_2\text{Cu}$  was prepared by arc-melting Mg–Cu (85.5:14.5) [38]. The sample was hydrogenated using two different methods, (a) ( $p(\text{H}_2) = 6$  bar and  $T = 325$  °C), and the low hydrogen pressure should facilitate the formation of  $\text{MgH}_2$ – $\text{Mg}_2\text{Cu}$  and (b), ( $p(\text{H}_2) = 30$  bar and  $T = 325$  °C) in order to facilitate the formation of  $\text{MgH}_2$ – $\text{MgCu}_2$ . The in situ SR-PXD results

[39] confirmed that the reversible alloy formed upon dehydrogenation. The apparent activation energy for the dehydrogenation of air-exposed  $\text{MgH}_2/\text{Mg}_2\text{Cu}$  and  $\text{MgH}_2/\text{MgCu}_2$  sample was found to be  $E_A \sim 108$  and  $\sim 160$  kJ/mol, respectively [39]. Furthermore, substantially improved dehydrogenation kinetics of  $\text{MgH}_2$  and resistance towards oxidation of Mg due to the presence of  $\text{Mg}_2\text{Cu}/\text{MgCu}_2$  is observed. The apparent activation energy found for dehydrogenation of  $\text{MgH}_2$  in  $\text{MgH}_2/\text{Mg}_2\text{Cu}$  is in agreement with previous work [38]. The activation energies extracted for the air-exposed samples may be assumed to be maximum values, which may be relevant to know for practical applications. This work also illustrates that in situ synchrotron radiation powder X-ray diffraction (SR-PXD) is a useful technique for investigation of kinetic properties [40, 41]. These results indicate that the presence of either  $\text{Mg}_2\text{Cu}$  or  $\text{MgCu}_2$  in  $\text{MgH}_2$  has a pronounced positive effect on the dehydrogenation kinetics of air-exposed samples.

In addition to diffusion of hydrogen, hydrogen cycling requires solid-state diffusion of Mg, transforming it from the Mg-poor to the Mg-rich state of the alloy and vice versa. Solid-state diffusion, and hence the hydrogen sorption reaction in this system, is rather slow. Hence, one of the areas of recent study is the effect of reducing particle sizes. Supported nanocrystallites with an average size of 20 nm were prepared by initial deposition of Cu nanoparticles followed by Mg deposition and hydrogenation [42]. The temperature for hydrogen desorption was  $\sim 150$  °C lower than for micron-sized material, and the kinetic performance was stable upon cycling. An activation energy for the hydrogen desorption of only 97 kJ/mol was found, clearly demonstrating the benefits of a reduction in particle size for the sorption kinetics, however at the expense of hydrogen storage capacity due to the carbon support.

### 1.3.3 Cobalt

The Mg–Co system contains only one intermetallic compound, a Laves-type  $\text{MgCo}_2$ . However, sintering of the mixtures of the fine metal powders of Mg and Co at 450–500 °C and hydrogen pressure (90 bar), or reactive ball-milling of the stoichiometric 2:1 mixtures of Mg and Co under hydrogen gas leads to the formation of  $\text{Mg}_2\text{CoH}_5$ .

Substitution of Fe in  $\text{Mg}_2\text{FeH}_6$  by Co results in the formation of  $\text{Mg}_2\text{CoH}_5$  with a smaller H/M ratio of 5/3 instead of 2.0, and with a much decreased thermal stability. Hydrogen desorption from  $\text{Mg}_2\text{CoH}_5$  is a multistep process, which at 500 °C leads to the formation of MgCo and Mg [43]. This process is, however, reversible and allows the synthesis of  $\text{Mg}_2\text{CoH}_5$  when the mixture MgCo + Mg is heated above 300 °C under a hydrogen pressure of 100 bar.

Hydrogenation of the  $\text{MgCo}_2$  intermetallic alloy has been tried at similar high-pressure conditions to those applied to  $\text{MgNi}_2$ . However, the metal sublattice becomes destabilized by Co which disproportionates to  $\text{Mg}_2\text{CoH}_5$  and Co. The solid-solution-type ternary alloys  $\text{MgNi}_{2-x}\text{Co}_x$  ( $x = 0.25; 0.5, \text{ and } 0.75$ ) also are unstable compared with disproportionation into  $\text{Mg}_2(\text{Ni},\text{Co})\text{H}_{5-x}$ , even with the smallest content of Co at  $x = 0.25$  (Antonov, Denys, Yartys, unpublished, 2015).

### 1.3.4 Titanium

Hydrogen storage behaviour of Mg nanoparticles (size range 100 nm to 1  $\mu\text{m}$ ) with metal-oxide core-shell morphology synthesized by inert gas condensation and decorated by titanium clusters via in situ vacuum deposition has been reported to improve only the kinetics [44]. Beside the alloying effect with transition metals, composite materials made of Mg with immiscible metals can also be prepared [36, 45]. Ponthieu et al. [46] investigated the Mg-Ti-H system focusing on  $\text{MgH}_2$ - $\text{TiH}_2$  nanocomposites. They observed that this mixture leads to materials exhibiting very fast sorption kinetics. The samples were prepared by ball-milling of various mixtures of Mg and Ti under hydrogen pressure. In this way, nanocomposites were prepared in the range  $x = 0$  to 0.5 for the system  $(1-x)\text{MgH}_2-x\text{TiH}_2$ . They consist of  $\text{MgH}_2$  (with the coexistence of  $\alpha$ - and  $\gamma$ -polymorphs) and  $\varepsilon$ - $\text{TiH}_2$  homogeneously distributed with crystallite sizes below 15 nm. A study of the sorption properties showed that only the magnesium hydride is reversible under moderate conditions ( $T < 330$  °C,  $p(\text{H}_2) < 1$  MPa), and the thermodynamics of the  $\text{Mg}/\text{MgD}_2$  equilibrium is not affected. However, the presence of the titanium hydride leads to very fast hydrogen sorption kinetics for the magnesium system. Indeed,  $\text{TiH}_2$  inclusions with particle sizes of 10 nm are found homogeneously distributed within the  $\text{MgH}_2$  matrix, and a coherent coupling between titanium hydride inclusions and the  $\text{Mg}/\text{MgD}_2$  matrix has been reported. This coupling is expected to enhance hydrogen mobility within the nanocomposite components as  $\text{TiH}_2$  inclusions limit grain growth of both Mg and  $\text{MgH}_2$  phases preserving short diffusion paths for hydrogen. Furthermore,  $\text{TiH}_2$  is expected to favour the diffusivity of hydrogen through the existence of coherent coupling between  $\text{TiH}_2$  and  $\text{Mg}/\text{MgH}_2$ . Though  $\text{TiH}_2$  does not influence the  $\text{Mg}/\text{MgD}_2$  thermodynamics, it provides fast sorption kinetics, allowing the nanocomposites to absorb large amounts of hydrogen at room temperature. These kinetic properties are attributed to the limited grain growth of Mg and  $\text{MgD}_2$  phases, the coherent coupling between  $\text{TiH}_2$  and  $\text{Mg}/\text{MgH}_2$ , and the fast H-diffusion through sub-stoichiometric  $\text{MgD}_{2-\eta}$  and  $\text{TiD}_{2-\eta}$  phases.

### 1.3.5 Palladium

The Mg-Pd phase diagram is rather complex and comprises several intermetallic phases. The  $\text{Mg}_6\text{Pd}$  phases have attracted most interest for hydrogen storage, as it is the lightest and least costly intermetallic. Mg-Pd composite nanoparticles were synthesized by inert gas condensation of Mg vapours followed by vacuum evaporation of Pd clusters. Formation of the  $\text{Mg}_6\text{Pd}$  intermetallic phase takes place upon vacuum annealing, resulting in  $\text{Mg}/\text{Mg}_6\text{Pd}$ , which transforms to different Mg-Pd intermetallic compounds upon hydrogen absorption, depending on temperature and pressure [47].

$\text{Mg}_6\text{Pd}$  nanoparticles of 4 nm were obtained by infiltration of Mg on previously formed Pd nanoparticles dispersed into the pores of porous carbon [48]. Mg infiltration resulted in the in situ formation of intermetallic  $\text{Mg}_6\text{Pd}$  nanoparticles. From the EXAFS-based structural analysis, it was demonstrated that the crystal structure of the nanoparticles is different than bulk  $\text{Mg}_6\text{Pd}$ . The nanoparticles exhibit a simpler crystallographic arrangement and a higher atomic disorder. As for the structural properties, thermodynamic and kinetic sorption properties also show different behaviours than for the bulk material. A change in the plateau pressure (Fig. 6) indicating thermodynamic destabilization of the hydride phase has been reported. In addition, faster kinetics were observed for the  $\text{Mg}_6\text{Pd}$  nanoparticles (Fig. 7) that remain stable for at least 10 sorption cycles though the particle size increased from 4 nm in the as-synthesized compound to 10 nm after hydrogenation. This modification of the sorption properties is related to the small particle size, as well as the difference in the crystal structure compared to that of bulk  $\text{Mg}_6\text{Pd}$ .

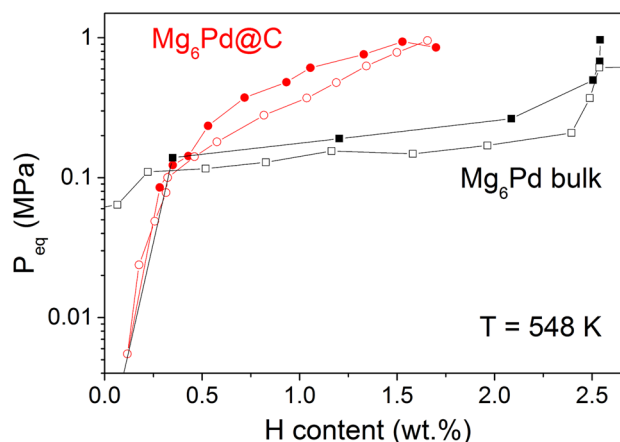


**Fig. 6** Hydrogen sorption isotherms at 275 °C for the bulk (black line) and nanoconfined (red line)  $\text{Mg}_6\text{Pd}$ . Full and empty symbols stand for absorption and desorption isotherm curves, respectively [48]

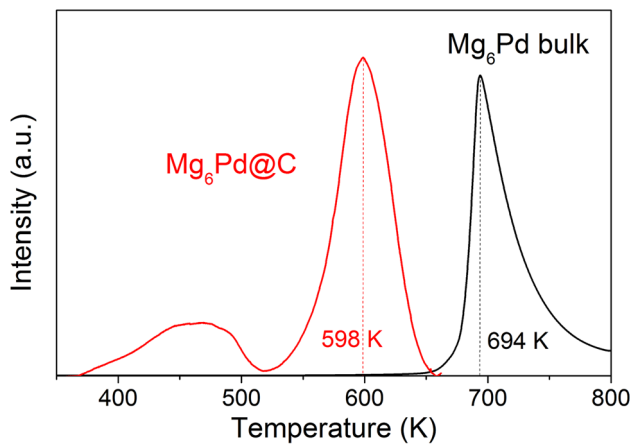
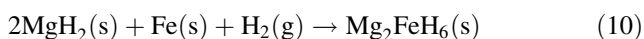


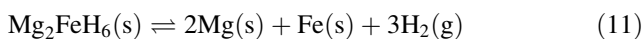
**Fig. 7** Thermal hydrogen desorption mass spectra of hydrogenated bulk (black line) and nanoconfined (red line)  $\text{Mg}_6\text{Pd}$  ( $m/e = 2$ , heating rate  $5^\circ\text{C}/\text{min}$ ) [48]

### 1.3.6 Iron

Magnesium iron hydride is known to have one of the highest volumetric hydrogen density of  $\rho_v = 150 \text{ g H}_2/\text{L}$ , moderate gravimetric storage density  $\rho_m = 5.47 \text{ wt\% H}$  and can be prepared from inexpensive chemicals [49–51]. The  $\text{Mg}_2\text{Fe}$  alloy is stabilized by hydrogen, i.e.  $\text{Mg}_2\text{FeH}_6$  forms in a reaction between magnesium hydride and iron at  $T > T_{\text{dec}}(\text{MgH}_2)$ . The reaction (Eq. 10) for a sample of  $\text{MgH}_2\text{--Fe}$  (2:1) in the temperature range  $380\text{--}470^\circ\text{C}$ ,  $p(\text{H}_2) = 100 \text{ bar}$ , was studied using in situ SR-PXD. The hydrogen pressure stabilizes the  $\text{MgH}_2$  and facilitates the reaction.



$\text{Mg}_2\text{FeH}_6$  was cooled to RT where it is stable and then heated in argon ( $p(\text{Ar}) = 1 \text{ bar}$ ). A series of in situ SR-PXD patterns revealed that  $\text{Mg}_2\text{FeH}_6$  apparently decomposes directly to the metals according to reaction (Eq. 11) in agreement with previous investigations and the fact that  $T_{\text{dec}}(\text{Mg}_2\text{FeH}_6) > T_{\text{dec}}(\text{MgH}_2)$ ,  $\Delta H_{\text{dec}}(\text{Mg}_2\text{FeH}_6) = 87 \pm 3 \text{ kJ/mol H}_2$  [52].



### 1.3.7 Zinc

$\text{Mg--Zn}$  alloys have been investigated for hydrogen storage but have not been found to improve the storage properties of Mg [52]. *Ex situ* X-ray diffraction has been used to show that the Zn forms an intermetallic alloy with Mg, which upon absorption of hydrogen either remains unaffected [52] or forms a higher Zn content intermetallic alloying more Mg to form a hydride [53, 54]. However, it has also been shown by in situ neutron diffraction that a Zn-containing

liquid phase forms at the temperatures typically used for hydrogenation [55]. No Zn hydride or Mg–Zn ternary hydride has been observed.

## 1.4 Mg-containing quasicrystals

Quasicrystals (QCs) are materials with long-range order but which lack three-dimensional translational periodicity. The first of these structures discovered was a rapidly solidified Al–Mn alloy [56]. Over a hundred binary and ternary QC intermetallic systems have been discovered; half of these are metastable and require rapid solidification production techniques, such as splat cooling or melt spinning [57]. The initial QC systems were mostly Al-based; however, Mg-containing QCs in the Mg–Zn–(Y, RE) system were reported by Luo et al. [58]. QC structures present the opportunity to develop new hydride systems, with unusual physical and mechanical properties [59] and high H/M ratios because there are more interstitial sites for hydrogen compared to conventional hydrides. A limited number of studies have explored the hydrogen storage properties of QC systems, most of which focus on Ti-based QCs, for example Ti–Zr–Ni and Ti–Hf–Ni. These achieved relatively high hydrogen storage capacities ( $H/M = 1.6$ ), but the recovery of the QC phase was difficult, due to the formation of  $\text{ZrH}_2$  or  $\text{TiH}_2$  and  $\text{Ti}_2\text{Ni}$  alloy after one (de)hydrogenation cycle [60, 61]. Sahlberg and Andersson [62] initially investigated the hydrogenation properties of a cubic  $\text{Mg}_3\text{Y}_2\text{Zn}_3$  ternary alloy with limited success. It only hydrogenated above  $400^\circ\text{C}$  and had a low hydrogen storage capacity (0.3 wt%).

More recently, Luo et al. [63] presented a study on the hydrogenation properties of a Zn–Mg–Y quasicrystal and its ternary alloys. The approximate stoichiometry of the stable Zn–Mg–Y icosahedral QC (i-phase) was confirmed to be  $\text{Zn}_{60}\text{Mg}_{30}\text{Y}_{10}$ . Three nominal compositions were prepared: ZMY-1,  $\text{Zn}_{50}\text{Mg}_{42}\text{Y}_8$  by gas atomization in an argon atmosphere; ZMY-2,  $\text{Zn}_{60}\text{Mg}_{30}\text{Y}_{10}$  by induction melting; and ZMY-3,  $\text{Zn}_{60}\text{Mg}_{30}\text{Y}_{10}$  by gas atomization followed by annealing at  $585^\circ\text{C}$ . The as-prepared samples were ball-milled under 1 bar Ar for 2 h. A quasicrystal i-phase was observed in all three as-prepared Zn–Mg–Y alloy samples, (Fig. 8). Despite using different preparation methods and initial nominal compositions, ZMY-1 and ZMY2 showed similar XRD patterns consisting of two major phases, i-phase and a H-phase (hexagonal  $(\text{Zn,Mg})_5\text{Y}$  alloy). Unlike the other two samples, ZMY-3 exhibited peaks only associated with the i-phase.

The SEM image of the as-prepared ZMY-1 sample (Fig. 9a) shows that spherical particles of sizes smaller than  $200 \mu\text{m}$  were formed through gas atomization, with a distinctive structure on the surface, while cross-sectional SEM backscattered electron (BSE) images of ZMY-1 and



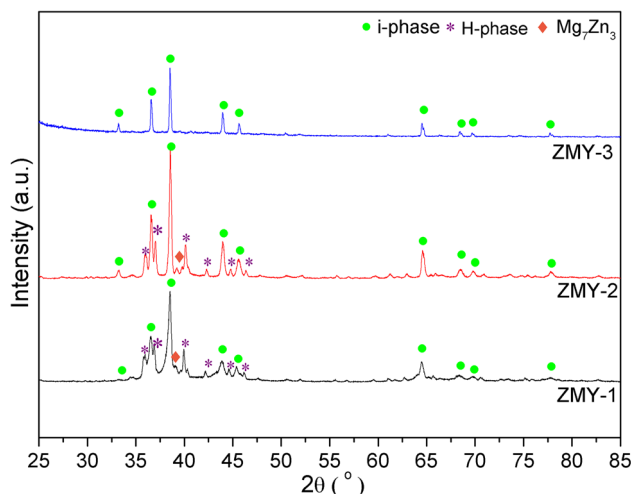


**Fig. 8** X-ray diffraction patterns of as-prepared Zn–Mg–Y samples. ZMY-1 and ZMY-2 consisted of three phases including a QC i-phase, H-phase, and  $Mg_7Zn_3$ , while the ZMY-3 sample consisted of a single i-phase [50]

ZMY-2 (Fig. 9b, c) indicated the presence of i-phase and H-phase in both samples, with different microstructures. ZMY-1 was formed of a petal-like i-phase surrounded by small white dots (ca. 1  $\mu m$ ) from the H-phase, while ZMY-2 consisted of dendritic H-phase structures located in the middle of the i-phase. The i-phase dominated ZMY-3, accounting for >95 % of the volume fraction based on cross-sectional BSE imaging.

The annealed Zn–Mg–Y QC sample (ZMY-3) had a 0.3 wt% hydrogen storage capacity and a high DSC decomposition temperature (503  $^{\circ}C$ ), while higher hydrogen storage capacity (0.9 wt%) and lower decomposition temperature (445  $^{\circ}C$ ) were achieved with ZMY-1, which had a greater H-phase contribution. The H-phase contains a greater proportion of Y that may cause the expansion of the unit cell and thus facilitate the hosting of more hydrogen atoms, as in ZMY-1. In addition, the lower decomposition temperature may be attributed to a smaller i-phase grain resulting in faster kinetics. TGA results showed that ZMY-1, ZMY-2, and ZMY-3 released  $1.0 \pm 0.1$ ,  $0.3 \pm 0.1$ , and  $0.4 \pm 0.1$  wt% of hydrogen, respectively, which was in close agreement with the PCI curves. A hydrogenation plateau (of ca. 3.5 bar) was observed on its PCI curve at 300  $^{\circ}C$  which suggests an improvement on the thermodynamics of  $MgH_2$  (1.4 bar at 300  $^{\circ}C$ ). Further work is required to investigate the (de)hydrogenation reaction mechanism and speed up the reaction kinetics.

### 1.5 RE–Mg–Ni hydrides (RE = La, Pr, Nd)

Despite significant differences in chemistry between the rare earth metals (RE) and magnesium, Mg forms extensive solid solutions in the  $RENi_3$  intermetallic alloys,

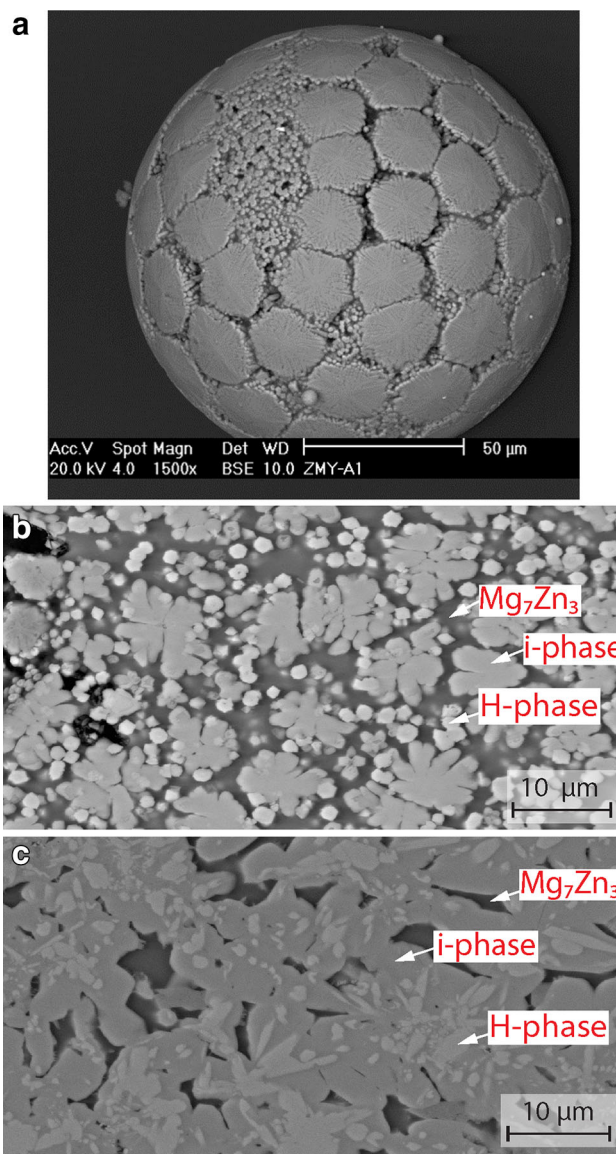


**Fig. 9** SEM backscattered electron (BSE) images of **a** surface as-prepared ZMY-1, **b** cross-sectional ZMY-1, and **c** cross-sectional ZMY-2 [50]

crystallizing with a  $PuNi_3$ -type trigonal structure. Up to 67 % of RE atoms can be replaced by Mg to form  $REMg_2Ni_9$  intermetallic compound. The  $RENi_3$  crystal structures are formed by a stacking of the  $RENi_5$  (*Haucke*  $CaCu_5$  type) and  $RENi_2$  (*Laves* type) slabs along the trigonal  $00z$  axis ( $RENi_5 + 2MgNi_2 = REMg_2Ni_9$ ). The substitution  $Mg \rightarrow RE$  takes place within the Laves-type slabs only leaving  $RENi_5$  layers unmodified ( $RENi_5 + 2MgNi_2 = REMg_2Ni_9$ ). In fact, a small yet significant replacement of RE by Mg (5 %) was observed in  $La_{0.91}Mg_{2.09}Ni_9$  within the  $AB_5$  slabs leading to the formation of the over-stoichiometric compositions  $RE_{1-x}Mg_{2+x}Ni_9$  crystallizing with  $PuNi_3$ -type structure.

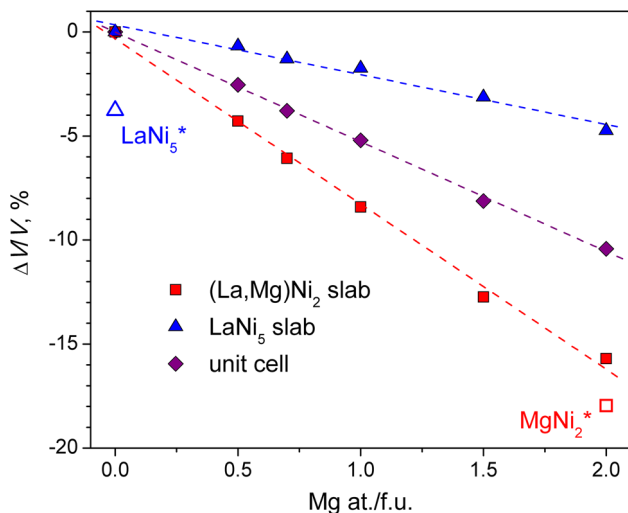


**Fig. 10** Relative changes in the volumes of the unit cells and constituent fragments of the  $\text{La}_{3-x}\text{Mg}_x\text{Ni}_9$  structures during the  $\text{Mg} \rightarrow \text{La}$  substitution. The data for the individual  $\text{LaNi}_5$  and  $\text{MgNi}_2$  compounds are given as a reference

A gradual increase in Mg content in  $\text{RE}_{3-x}\text{Mg}_x\text{Ni}_9$  is accompanied by a linear decrease in the volumes of the unit cells (Fig. 10). Interestingly, a substantial contraction takes place not only for the  $(\text{RE},\text{Mg})_2\text{Ni}_4$  slabs, but also for Mg-free  $\text{CaCu}_5$ -type  $\text{RENi}_5$  slabs [64].

Magnesium significantly affects the bonding mechanism of metal–hydrogen interactions studied in detail for  $\text{La}_2\text{MgNi}_9$ -based hydride [65]. A prominent and the most important feature of the structure of  $\text{La}_2\text{MgNi}_9\text{D}_{13}$  is in the local ordering of the hydrogen sublattice built by stacking of the  $\text{MgH}_6$  octahedra and  $\text{NiH}_4$  tetrahedra (Fig. 11).

Substitution of the largest (in size) atom of the rare earth metals—lanthanum—by smaller atoms like Pr or Nd leads to the contraction of the volumes of the unit cells of  $(\text{La},\text{Pr},\text{Nd})_2\text{MgNi}_9$ , reaching 2.6 % for  $\text{Nd}_2\text{MgNi}_9$  [66]. The hydrogen storage capacity of the alloys remains unchanged, 12–13 at. $\text{H}/\text{f.u.}(\text{La},\text{Pr},\text{Nd})_2\text{MgNi}_9$ . However, shrinking of the lattice quite significantly affects the thermodynamic stability of the formed hydrides. As evident from the room-temperature isotherms (Fig. 12), equilibrium pressures of both hydrogen absorption and desorption in the  $\text{Nd}_2\text{MgNi}_9\text{-H}_2$  system are an order of magnitude higher than in the  $\text{La}_2\text{MgNi}_9\text{-H}_2$  system changing from  $<0.1$  bar for the  $\text{La}_2\text{MgNi}_9$ -based hydride to  $>1$  bar for  $\text{Nd}_2\text{MgNi}_9\text{H}_{12}$ .

The properties of  $\text{RE}_{3-x}\text{Mg}_x\text{Ni}_9$ -based hydrides dramatically change when the content of magnesium extends to the maximum solubility limit, close to two atoms of Mg/f.u. for  $\text{RE}_{3-x}\text{Mg}_x\text{Ni}_9$ . In situ neutron powder diffraction studies of two deuterides  $\text{La}_{1.09}\text{Mg}_{1.91}\text{Ni}_9\text{D}_{9.5}$  and  $\text{La}_{0.91}\text{Mg}_{2.09}\text{Ni}_9\text{D}_{9.4}$  performed at deuterium pressures reaching 918 bar  $\text{D}_2$  showed that the hydrogenation properties of Mg-rich

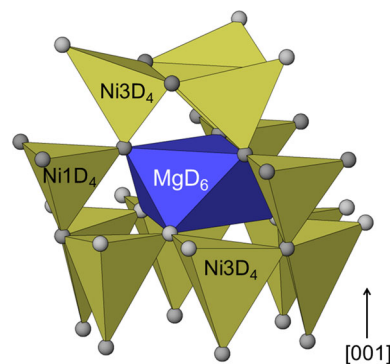


**Fig. 11** Hydrogen sublattice for the  $\text{La}_2\text{MgNi}_9\text{D}_{13}$  structure. The sublattice is formed by the stacking of  $\text{MgD}_6$  octahedra and  $\text{NiD}_4$  tetrahedra. Such stacking gives an irregular, buckled framework

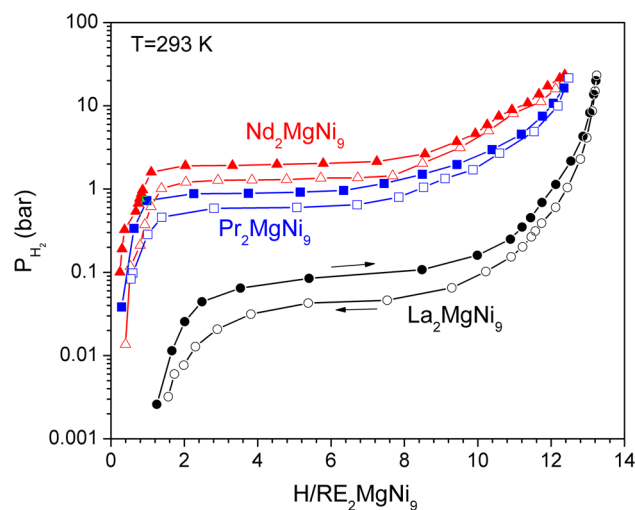


**Fig. 12** PCT diagrams for  $\text{Nd}_2\text{MgNi}_9\text{-H}_2$ ,  $\text{Pr}_2\text{MgNi}_9\text{-H}_2$ , and  $\text{La}_2\text{MgNi}_9\text{-H}_2$  systems

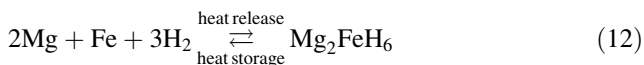
compounds are principally different from those for  $\text{LaNi}_3$  [67].  $\text{LaNi}_5$ -assisted hydrogenation of  $\text{MgNi}_2$  in the hybrid structure of  $\text{LaMg}_2\text{Ni}_9$  takes place. In the deuterides, the D atoms are accommodated in both Laves- and  $\text{CaCu}_5$ -type slabs. The overall chemical compositions can be presented as  $\text{LaNi}_5\text{H}_{5.6/5.0} + 2 * \text{MgNi}_2\text{H}_{1.95/2.2}$  showing that the hydrogenation of the  $\text{MgNi}_2$  slab proceeds at mild  $\text{H}_2/\text{D}_2$  pressure of just 20 bar. A partial filling by D of the four types of the tetrahedral interstices in the  $\text{MgNi}_2$  slab takes place, including  $[\text{MgNi}_3]$  and  $[\text{Mg}_2\text{Ni}_2]$  tetrahedra. Magnesium causes a significant destabilization of the hydrides;  $\text{La}_{1.09}\text{Mg}_{1.91}\text{Ni}_9$  reversibly forms hydrides with  $\Delta H_{\text{des}} = 24.0$  kJ/mol  $\text{H}_2$  (as compared to  $\Delta H_{\text{des}} = 35.9$  kJ/mol  $\text{H}_2$  for  $\text{La}_2\text{MgNi}_9$  [66]) and an equilibrium pressure of  $\text{H}_2$  desorption of 18 bar at 20 °C (0.05 bar at 20 °C for  $\text{La}_2\text{MgNi}_9$  [65]). However, magnesium also introduces a pronounced hysteresis of  $\text{H}_2$  absorption and desorption,  $\sim 100$  bar. The latter is probably caused by a huge

difference in the dimensions of the Ni net in the individual crystal lattices of  $\text{MgNi}_2$  and  $\text{LaNi}_5$ .

### 1.6 Magnesium compounds for high-temperature energy storage

Thermochemical gas–solid reactions are suitable as long-term or short-term heat storage systems. Important for short-term heat storage systems is good kinetics of the absorption and desorption of the gaseous compound combined with good heat conductivity of the reaction bed. After separation of both compounds during the decomposition process, all of this energy is trapped in the system and can be used at any time without energy losses (long-term storage). Reversible Mg-based metal hydride systems show a rather high range of energy densities (62–77 kJ/mol  $\text{H}_2$ ; see Table 1) making their use convenient in thermochemical heat storage systems, even though the values 62–77 kJ/mol  $\text{H}_2$  are significantly lower as compared to the highest observed values for the metal hydrides,  $\text{YH}_{1.8}$  (220 kJ/mol  $\text{H}_2$ ),  $\text{ZrH}_{1.6}$  (212 kJ/mol  $\text{H}_2$ ) and  $\text{CaH}_2$  (207.7 kJ/mol  $\text{H}_2$ ) [68].

While research in past years has been focused on the pure Mg/ $\text{MgH}_2$  system, which can be used for temperatures up to 400 °C in solar power parabolic trough systems, new developments now focus on the 2 Mg + Fe/ $\text{Mg}_2\text{FeH}_6$  system. This material can be used at temperatures up to 550 °C as a possible heat storage material for the solar tower power plants and shows excellent stability over hundreds of hydrogenation and dehydrogenation cycles (Eq. 12).



Current research is focused on the identification of cost-effective materials undergoing hydrogenation–dehydrogenation reactions (heat storage–heat release) with a high degree of reversibility upon multiple cycles and fast and controllable kinetics [69]. A wide range of temperatures with different Mg-based metal hydrides between 400 and 600 °C can be covered.

### 1.7 The HDDR processes in the Mg-based alloys ( $\text{LaMg}_{12}$ , $\text{LaMg}_{11}\text{Ni}$ )

The hydrogenation–disproportionation–desorption–recombination (HDDR) process includes two stages of hydrogen absorption, normally at relatively lower and higher temperatures promoting, respectively, the formation of interstitial hydrides with expanded cells and the disproportionation of the metallic matrix of this hydride accompanied by the formation of binary hydrides and other phases with reduced (zero) content of the hydride-forming element, e.g. the products of disproportionation.

The high-temperature desorption of hydrogen is accompanied by the recombination of the source compound but already with sub-micrometre grain sizes. For the magnesium-rich compounds of rare earth metals, because of a very large enthalpy of formation of both  $\text{MgH}_2$  (−74 kJ/mol  $\text{H}_2$ ) and rare earth metals (−208 kJ/mol  $\text{H}_2$  for  $\text{LaH}_2$ ), the formation of the interstitial-type hydrides becomes thermodynamically unfavourable as compared to the formation of the hydrides of Mg and rare earth metals. However, even though the decomposition of the rare earth hydrides needs application of extremely high temperatures, more than 800 °C (in vacuum) for  $\text{LaH}_2$ , it becomes destabilized by magnesium metal formed during hydrogen desorption from  $\text{MgH}_2$ . This makes possible a recombination of the intermetallics of rare earths and magnesium below 450 °C. The latter temperature is 400 °C lower than the temperature required to decompose individual  $\text{LaH}_2$ .

In the case of  $\text{LaMg}_{12}$ , hydrogen absorption resulted in a two-step disproportionation process:  $\text{LaMg}_{12} + \text{H}_2 \rightarrow \text{LaH}_3 + \text{Mg} \rightarrow \text{LaH}_3 + \text{MgH}_2$  [33]. It is interesting that instead of immediate formation of  $\text{MgH}_2$ , the magnesium metal was formed first, before interacting with hydrogen to yield a magnesium dihydride.

A decrease in the grain size of the initial alloy was achieved by applying a rapid solidification (RS) process, and this was found to assist in improving the hydrogenation kinetics. It is interesting to note that ribbons of the RS samples retained their initial shapes after the hydrogenation despite the fact that formation of  $\text{LaH}_3$  and  $\text{MgH}_2$  hydrides is accompanied by a significant volume expansion.

Hydrogen thermal desorption in vacuum occurred in different ways for the alloys solidified at different quenching rates. A major peak of hydrogen evolution was located at ~370 °C; however, for the alloys synthesized by rapid solidification and having the smallest grain size, an extra desorption event was observed at 415 °C (Fig. 13). SR XRD study showed that this extra peak is associated with Mg-assisted low-temperature hydrogen desorption from  $\text{LaH}_2$  proceeding below 450 °C and leading to a recombination process to form the initial intermetallic alloy  $\text{LaMg}_{12}$ .

The chemical equations taking place in these two processes can be described as follows:

1. Desorption without recombination (RS samples prepared at low solidification rate and as-cast samples)
 
$$\text{MgH}_2 + \text{LaH}_3 \rightarrow \text{Mg} + \text{LaH}_2 + 3/2\text{H}_2$$
2. Desorption followed by recombination of  $\text{LaMg}_{12}$  (RS samples prepared at high solidification rate)
 
$$12\text{MgH}_2 + \text{LaH}_3 \rightarrow 12\text{Mg} + \text{LaH}_2 + 25/2\text{H}_2$$

$$\rightarrow \text{LaMg}_{12} + \text{H}_2$$



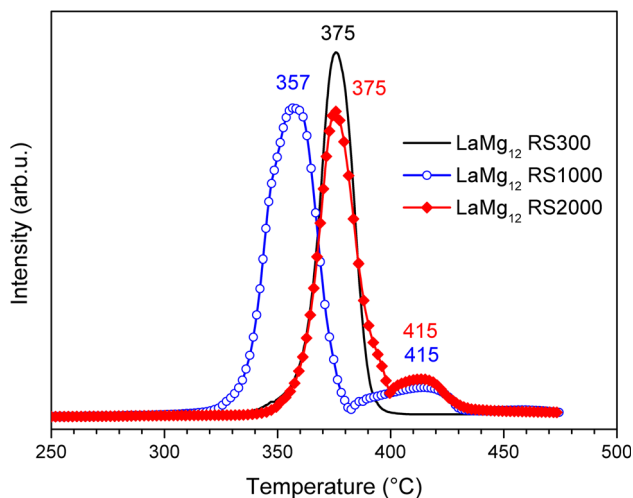


**Fig. 13** Hydrogen thermal desorption mass spectra of the hydrogenated RS alloys measured in vacuum

SEM studies revealed significant differences between the samples after completion of the thermal desorption of hydrogen. Samples for which the recombination stage was observed were found to have extremely porous morphology (pore sizes 0.5–2  $\mu\text{m}$ ; see Fig. 14). Such dramatic microstructural changes can be attributed to the recombination of the  $\text{LaMg}_{12-x}$  intermetallic during H desorption and associated with volume shrinkage during the

$\text{Mg} + \text{LaH}_2 \rightarrow \text{LaMg}_{12-x} + \text{H}_2$  transformation. No such transformation took place in the RS samples prepared at low solidification rate and the as-cast samples, which is attributed to their coarse initial microstructures. These observations show that fine nanostructuring of the material leads to a complete recombination process and to the enhancement of hydrogen exchange.

From comparison of the data for  $\text{LaMg}_{12}$  [33] with the results for the rapidly solidified  $\text{LaMg}_{11}\text{Ni}$  alloy where 1/12 of Mg was substituted by Ni [34, 35], it has been concluded that Ni substitution in combination with rapid solidification significantly improves the hydrogenation–desorption properties of the alloy leading to a dramatic increase in the rates of hydrogenation–dehydrogenation processes as a result of the nanostructuring of the samples and because of the catalytic influence of the formed  $\text{Mg}_2\text{Ni}$  intermetallics. On hydrogen desorption, the presence of mobile hydrogen in the metal lattice allows a low-temperature diffusion of both lanthanum and magnesium to proceed. Because of the thermodynamic advantage of the formation of La–Mg intermetallics compared to the mixture of Mg metal and lanthanum dihydride, this causes a recombination reaction to proceed below 450  $^{\circ}\text{C}$ , 400  $^{\circ}\text{C}$  lower than the decomposition temperature of  $\text{LaH}_2$ , to sequentially form  $\text{LaMg}_{12-x}$ , and later,  $\text{La}_2\text{Mg}_{17}$  intermetallics (Fig. 15).

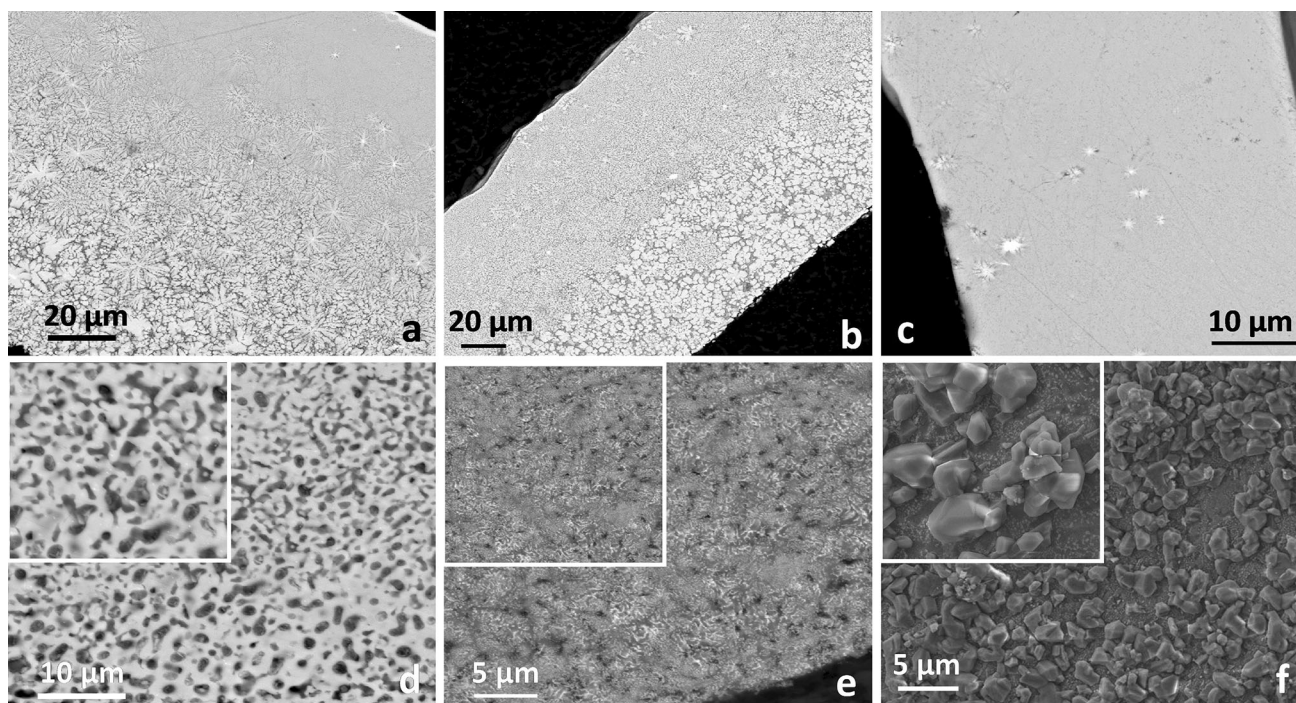
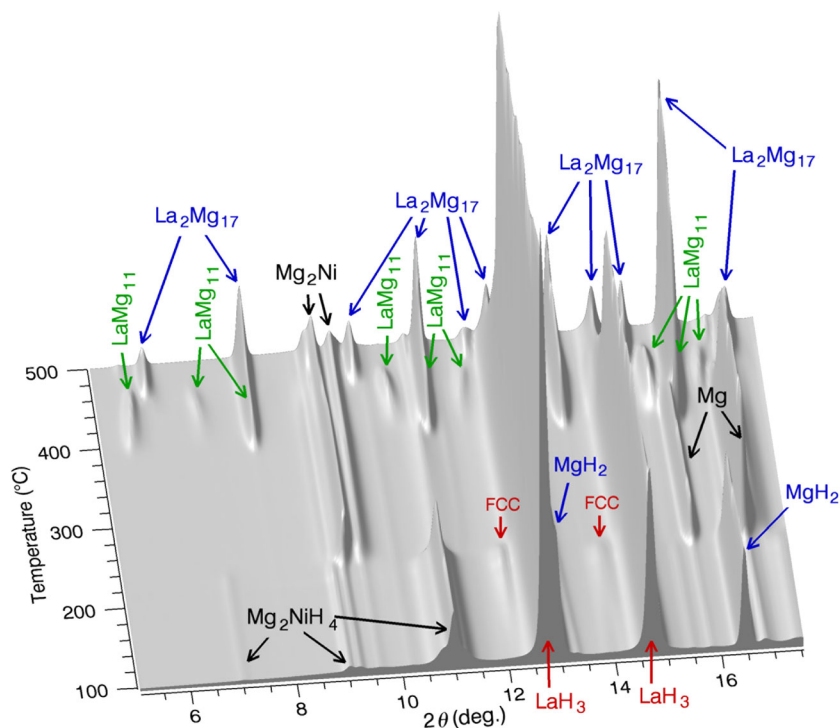


**Fig. 14** Backscattered SEM images of the RS  $\text{LaMg}_{12}$  samples (a RS300; b RS1000; c RS2000) and RS2000 sample at different stages of hydrogen processing (d after TDS from the hydride; e, after

five hydrogen absorption–desorption cycles; f hydrogenated sample). For the inserted magnified square areas, the sides are 5  $\mu\text{m}$

**Fig. 15** Evolution of the in situ SR XRD pattern from the hydrogenated  $\text{LaMg}_{11}\text{Ni}$  alloy during hydrogen vacuum thermal desorption in the temperature range 100–500 °C (heating rate 2 °C/min; SNBL BM01A;  $\lambda = 0.72085 \text{ \AA}$ ). Peaks marked FCC correspond to a LaHO oxyhydride



Ribbons of the RS samples retained their initial shapes despite the fact that formation of  $\text{LaH}_3$  and  $\text{MgH}_2$  hydrides is accompanied by a significant volume expansion.

## 2 First-principle study on Mg-based hydrides

Between interstitial metal hydrides, such as  $\text{LaNi}_5\text{H}_6$ , and ionic complexes, such as  $\text{Mg}_2\text{NiH}_4$ , a large family of (La,Mg)-Ni hydrides exists, exhibiting intermediate electronic properties. The host intermetallics belong to the  $(\text{La,Mg})\text{Ni}_y$  family, with  $y = (5n + 4)/(n + 2)$ . It has been shown [70] that such intermetallics are stabilized by the stacking along the  $c$ -axis of  $n * [\text{LaNi}_5] + m * [\text{LaMgNi}_4]$  layers of *Haucke* and *Laves* phases, respectively, with Mg atoms occupying only half La sites of the latter. In this context, a systematic investigation of the electronic properties of the  $(\text{La,Mg})_2\text{Ni}_7\text{H}_x$  hydrides has been recently done [71]. To understand the preferential interstitial H sites, a systematic comparison of 13 different sites showed that both geometrical and chemical factors govern the stability of the hydrides of the RE–Mg–Ni family. It has been shown that the calculated site preferences are in agreement with the experimental data, for which H occupies  $[\text{La}_2\text{Ni}_4]$  slab in  $\text{La}_2\text{Ni}_7$  compound mainly for geometrical reasons, whereas H goes in both  $[(\text{La,Mg})_2\text{Ni}_4]$  and  $[\text{LaNi}_5]$  slabs for the Mg-substituted compound driven by both geometrical and chemical factors. The  $\text{La}_{1.5}\text{Mg}_{0.5}\text{Ni}_7$  hydrides show electronic charge transfer from La

and Mg to H. Depending on the H site environment, the Bader charge analysis gives a value of about  $-0.31e$  on H, which classifies these hydrides as conventional metallic ones, such as  $\text{LaNi}_5\text{H}_x$ .

Another interesting study on Mg-based hydrides has been recently published on the trihydride  $\text{MgNi}_2\text{H}_3$  [36, 72]. The DFT calculations showed the formation of an electronic structure around  $-10$  to  $-6 \text{ eV}$  caused by the chemical bonds of hydrogen and its  $1s$  states mainly via interaction with the Ni  $3d$  states. The bonding mechanism is dominated by the formation of covalent bonds between Ni and H and a charge transfer from Mg to the two different H atoms which leads to a significant degree of ionic bonding between Mg ( $+1.59e$ ) and H ( $-0.55e$ ,  $-0.31e$ ). The calculated enthalpy of formation of  $\text{MgNi}_2\text{H}_3$  is approximately  $-30 \text{ kJ/mol H}_2$ , which is consistent with the stability of a hydride at normal conditions. Moreover, the analysis of calculated phonon dispersion curves has confirmed that the structure is mechanically stable in *Cmca* symmetry (Fig. 16), the most stable one among all considered alternatives. In addition, the thermodynamic properties of  $\text{MgNi}_2\text{H}_3$  with temperature and volume dependence have been estimated in the frame of the quasiharmonic approximation.

The variety of chemical bondings within Mg-based hydrides is illustrated in Fig. 17, showing the electron localization function (ELF) representations for several compounds. The probability function ranges between 0 (no probability) and 1 (perfect localization) for the valence



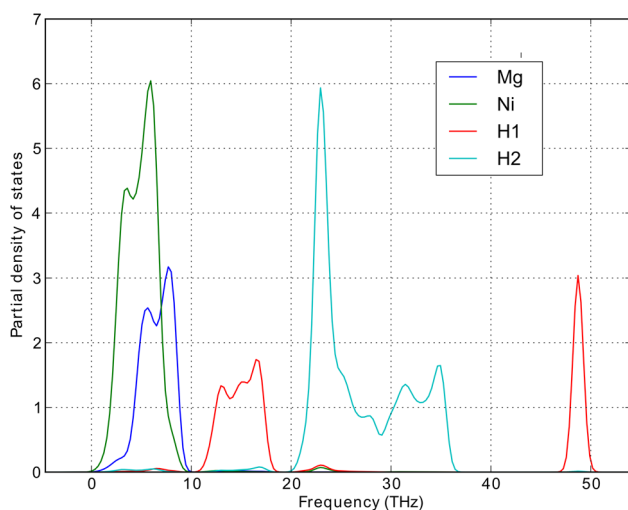
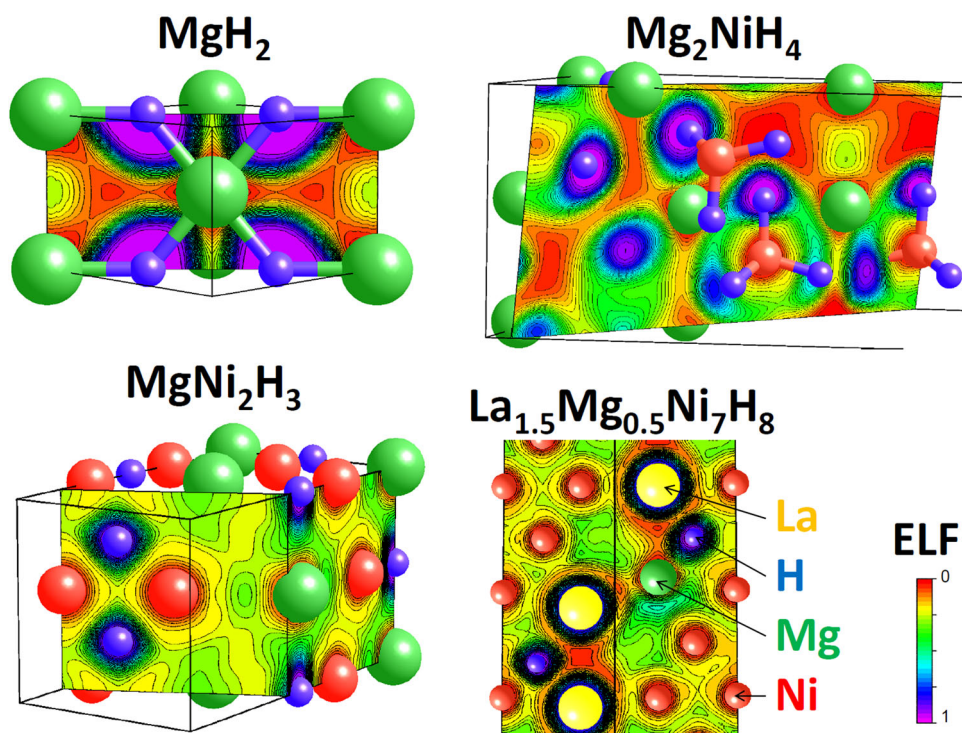


**Fig. 16** Partial phonon density of state (DOS) of  $\text{MgNi}_2\text{H}_3$  in the  $Cmca$  space group

electrons, 0.5 indicating probability similar to electron gas. Whereas  $\text{MgH}_2$  and  $\text{Mg}_2\text{NiH}_4$  show isolated anions around H atoms with a partial negative charge, and tetrahedral  $[\text{NiH}_4]^{2-}$  complex, respectively, the hydrides  $\text{La}_{1.5}\text{Mg}_{0.5}\text{Ni}_7\text{H}_x$  and  $\text{MgNi}_2\text{H}_3$  exhibit a non-null ELF region ( $>0.25$ ) between Mg and H. This behaviour fully shows that the partial covalent interaction between Mg and H is typical for a variety of magnesium-containing hydrides.

**Fig. 17** Electron localization function (ELF) images of selected planes containing Mg and H atoms into  $\text{MgH}_2$  ( $P4_2/mmm$ ),  $\text{Mg}_2\text{NiH}_4$  ( $C12$ ),  $\text{MgNi}_2\text{H}_3$  ( $Cmca$ ), and  $\text{La}_{1.5}\text{Mg}_{0.5}\text{Ni}_7\text{H}_8$  ( $P6_3/mmc$ )



### 3 Concluding remarks

Magnesium-based compounds continue to be the subject of intensive research for hydrogen storage, due to their light weight and inexpensive availability of magnesium. Practical limitations on the application for the pure metal, such as slow kinetics and high temperatures of desorption, require the development of compound materials to overcome these limitations. While improvements in kinetics have been achieved with nanostructuring processes, such as ball-milling, rapid solidification and other processes that introduce defects, and combination with relatively small amounts ( $<10$  wt%) of additives [8], improvements in the thermodynamics are necessary to substantially reduce dehydrogenation temperatures. Alloys and intermetallic compounds of magnesium provide a way of reducing the enthalpy of the reaction compared to the pure metal hydride.

A large number of materials, mostly metals, have been used to form magnesium compounds and the thermodynamics of their interaction with hydrogen has been characterized. In many cases, the new hydrogenated compounds have reduced enthalpies; however, problems such as slower kinetics, instability, and disproportionation upon hydrogen cycling often arise. Sometimes the preparation process introduces metastable phases that, although beneficial to the interaction with hydrogen, are lost after

the initial hydrogen cycling. In addition, the introduction of another material to the magnesium typically results in a reduction in hydrogen capacity.

Binary compounds of magnesium have been investigated quite thoroughly, and it may be that the feasible alloys for effective, low-temperature hydrogen storage materials have been exhausted. Ternary and higher alloys may offer new possibilities in this area.

Finally, a new area of use of the Mg-based hydrogenated compounds appears to be heat storage. Here, for the entire range of temperatures, future research will include the identification of the most promising candidates together with the synthesis and the full thermodynamic/thermophysical and kinetics characterization [73]. Moreover, hydrides working at relatively low equilibrium pressure (between 1 and 50 bar) and at a certain selected temperature will be preferred in order to minimize the complexity and the cost of the thermal energy storage system.

The present special issue contains two other closely related papers which could be of interest for the readers entitled “Review of magnesium hydride based materials: development and optimisation” [74] and “Integrated with FC H storage systems utilising magnesium hydride: experimental Studies and modelling” [75].

**Acknowledgments** This work is a part of the activities within IEA Task 32 Hydrogen-based Energy Storage. We are grateful for the operating agent Dr. Michael Hirscher and all the experts from the Task 32 for the fruitful collaboration.

## References

- M.B. Ley, L.H. Jepsen, Y.-S. Lee, Y.W. Cho, J.M. Bellosta von Colbe, M. Dornheim, M. Rokni, J.O. Jensen, M. Sloth, Y. Filinchuk, J.E. Jørgensen, F. Besenbacher, T.R. Jensen, Complex hydrides for hydrogen storage—new perspectives. *Mater. Today* **17**(3), 122–128 (2014)
- U. Eberle, M. Felderhoff, F. Schüth, Chemical and physical solutions for hydrogen storage. *Angew. Chem. Int. Ed.* **48**(36), 6608–6630 (2009)
- M. Dornheim, S. Doppiu, G. Barkhordarian, U. Boesenberg, T. Klassen, O. Gutfleisch, R. Bormann, Hydrogen storage in magnesium-based hydrides and hydride composites. *Scr. Mater.* **56**(10), 841–846 (2007)
- A. Zaluska, L. Zaluski, J.O. Ström-Olsen, Nanocrystalline magnesium for hydrogen storage. *J. Alloys Compd.* **288**(1–2), 217–225 (1999)
- J. Huot, G. Liang, R. Schulz, Mechanically alloyed metal hydride systems. *Appl. Phys. A Mater. Sci. Process.* **72**(2), 187–195 (2001)
- K. Alsabawi, T.A. Webb, E.M. Gray, C.J. Webb, Effect of C<sub>60</sub> Additive on Magnesium Hydride for Hydrogen Storage. *Int. J. Hydrog. Energy* **40**(33), 10508–10515 (2015)
- S. Bouaricha, J.P. Dodelet, D. Guay, J. Huot, R. Schulz, Study of the activation process of Mg-based hydrogen storage materials modified by graphite and other carbonaceous compounds. *J. Mater. Res.* **16**(10), 2893–2905 (2011)
- C.J. Webb, A review of catalyst-enhanced magnesium hydride as a hydrogen storage material. *J. Phys. Chem. Solids* **84**, 96–106 (2015)
- M. Paskevicius, D.A. Sheppard, K. Williamson, C.E. Buckley, Metal hydride thermal heat storage prototype for concentrating solar thermal power. *Energy* **88**, 469–477 (2015)
- A. Reiser, B. Bogdanovic, K. Schlichte, The application of Mg-based metal-hydrides as heat energy storage systems. *Int. J. Hydrog. Energy* **25**(5), 425–430 (2000)
- D.A. Sheppard, M. Paskevicius, C.E. Buckley, Thermodynamics of hydrogen desorption from NaMgH<sub>3</sub> and its application as a solar heat storage medium. *Chem. Mater.* **23**(19), 4298–4300 (2011)
- G.S. Walker, Multicomponent hydrogen storage systems, in *Solid-state Hydrogen Storage*, ed. by G.S. Walker (Woodhead Publishing Ltd, Cambridge, 2008), pp. 478–499
- J.J. Vajo, F. Mertens, C.C. Ahn, R.C. Bowman, B. Fultz, Altering hydrogen storage properties by hydride destabilization through alloy formation: LiH and MgH<sub>2</sub> destabilized with Si. *J. Phys. Chem. B* **108**(37), 13977–13983 (2004)
- R. Janot, F. Cuevas, M. Lacroche, A. Percheron-Guégan, Influence of crystallinity on the structural and hydrogenation properties of Mg<sub>2</sub>X phases (X = Ni, Si, Ge, Sn). *Intermetallics* **14**(2), 163–169 (2006)
- J. Zhang, Z. Li, F. Cuevas, M. Lacroche, Phase stabilities in the Mg–Si–H system tuned by mechanochemistry. *J. Phys. Chem. C* **118**(38), 21889–21895 (2014)
- A.-L. Chaudhary, M. Paskevicius, D.A. Sheppard, C.E. Buckley, Thermodynamic destabilisation of MgH<sub>2</sub> and NaMgH<sub>3</sub> using Group IV elements Si, Ge or Sn. *J. Alloys Compd.* **623**, 109–116 (2015)
- M. Paskevicius, D.A. Sheppard, A.L. Chaudhary, C.J. Webb, E.M.A. Gray, H.Y. Tian, V.K. Peterson, C.E. Buckley, Kinetic limitations in the Mg–Si–H system. *Int. J. Hydrog. Energy* **36**(17), 10779–10786 (2011)
- A.-L. Chaudhary, D.A. Sheppard, M. Paskevicius, C.J. Webb, E.M. Gray, C.E. Buckley, Mg<sub>2</sub>Si nanoparticle synthesis for high pressure hydrogenation. *J. Phys. Chem. C* **118**(2), 1240–1247 (2014)
- J. Bystrzycki, T. Płociński, W. Zieliński, Z. Wiśniewski, M. Polanski, W. Mróz, Z. Bojar, K.J. Kurzdłowski, Nano-engineering of magnesium hydride for hydrogen storage. *Microelectron. Eng.* **86**(4–6), 889–891 (2009)
- G.S. Walker, M. Abbas, D.M. Grant, C. Udeh, Destabilisation of magnesium hydride by germanium as a new potential multicomponent hydrogen storage system. *Chem. Commun.* **47**(28), 8001 (2011)
- F.C. Gennari, F.J. Castro, G. Urretavizcaya, G. Meyer, Catalytic effect of Ge on hydrogen desorption from MgH<sub>2</sub>. *J. Alloys Compd.* **334**(1–2), 277–284 (2002)
- Abbas M. Thermodynamic Tuning of Light Metal Hydrides Multicomponent Systems by Ge [PhD Thesis]. University of Nottingham; 2014
- M. Polanski, J. Bystrzycki, The influence of different additives on the solid-state reaction of magnesium hydride (MgH<sub>2</sub>) with Si. *Int. J. Hydrog. Energy* **34**(18), 7692–7699 (2009)
- A. Andreasen, M.B. Sørensen, R. Burkarl, B. Møller, A.M. Molenbroek, A.S. Pedersen, J.W. Andreasen, M.M. Nielsen, T.R. Jensen, Interaction of hydrogen with an Mg–Al alloy. *J. Alloys Compd.* **404–406**, 323–326 (2005)
- J.F. Fernández, C.R. Sánchez, Rate determining step in the absorption and desorption of hydrogen by magnesium. *J. Alloys Compd.* **340**(1–2), 189–198 (2002)
- J.F. Fernández, C.R. Sánchez, Simultaneous TDS–DSC measurements in magnesium hydride. *J. Alloys Compd.* **356–357**, 348–352 (2003)

27. G. Friedlmeier, M. Arakawa, T. Hirai, E. Akiba, Preparation and structural, thermal and hydriding characteristics of melt-spun Mg–Ni alloys. *J. Alloys Compd.* **292**(1–2), 107–117 (1999)
28. E. Callini, L. Pasquini, T.R. Jensen, E. Bonetti, Hydrogen storage properties of Mg–Ni nanoparticles. *Int. J. Hydrog. Energy* **38**(27), 12207–12212 (2013)
29. A. Zaluska, L. Zaluski, J.O. Ström-Olsen, Synergy of hydrogen sorption in ball-milled hydrides of Mg and Mg<sub>2</sub>Ni. *J. Alloys Compd.* **289**(1–2), 197–206 (1999)
30. S. Orimo, Structural and hydriding properties of the Mg–Ni–H system with nano- and/or amorphous structures. *Acta Mater.* **45**(6), 2271–2278 (1997)
31. J. Matsuda, N. Uchiyama, T. Kanai, K. Harada, E. Akiba, Effect of Mg/Ni ratio on microstructure of Mg–Ni films deposited by magnetron sputtering. *J. Alloys Compd.* **617**, 47–51 (2014)
32. J. Matsuda, K. Yoshida, Y. Sasaki, N. Uchiyama, E. Akiba, In situ observation on hydrogenation of Mg–Ni films using environmental transmission electron microscope with aberration correction. *Appl. Phys. Lett.* **105**(8), 083903 (2014)
33. R. Bogerd, P. Adelhelm, J.H. Meeldijk, K.P. de Jong, P.E. de Jongh, The structural characterization and H<sub>2</sub> sorption properties of carbon-supported Mg<sub>1–x</sub>Ni<sub>x</sub> nanocrystallites. *Nanotechnology* **20**(20), 204019 (2009)
34. Y. Wu, M.V. Lototsky, J.K. Solberg, V.A. Yartys, Effect of microstructure on the phase composition and hydrogen absorption–desorption behaviour of melt-spun Mg–20Ni–8Mm alloys. *Int. J. Hydrog. Energy* **37**(2), 1495–1508 (2012)
35. S. Løken, J.K. Solberg, J.P. Maehlen, R.V. Denys, M.V. Lototsky, B.P. Tarasov, V.A. Yartys, Nanostructured Mg–Mm–Ni hydrogen storage alloy: structure–properties relationship. *J. Alloys Compd.* **446–447**, 114–120 (2007)
36. V.A. Yartys, V.E. Antonov, D. Chernyshov, J.C. Crivello, R.V. Denys, V.K. Fedotov, M. Gupta, V.I. Kulakov, M. Latroche, D. Sheptyakov, Structure and chemical bonding in MgNi<sub>2</sub>H<sub>3</sub> from combined high resolution synchrotron and neutron diffraction studies and ab initio electronic structure calculations. *Acta Mater.* **98**, 416–422 (2015)
37. J.J. Reilly, R.H. Wiswall, Reaction of hydrogen with alloys of magnesium and copper. *Inorg. Chem.* **6**(12), 2220–2223 (1967)
38. A. Karty, Hydriding and dehydriding kinetics of Mg in a Mg/Mg<sub>2</sub>Cu eutectic alloy: pressure sweep method. *J. Appl. Phys.* **50**(11), 7200 (1979)
39. A. Andreasen, M.B. Sørensen, R. Burkarl, B. Møller, A.M. Molenbroek, A.S. Pedersen, T. Vegge, T.R. Jensen, Dehydrogenation kinetics of air-exposed MgH<sub>2</sub>/Mg<sub>2</sub>Cu and MgH<sub>2</sub>/MgCu<sub>2</sub> studied with in situ X-ray powder diffraction. *Appl. Phys. A* **82**(3), 515–521 (2006)
40. K.T. Møller, B.R.S. Hansen, A.-C. Dippel, J.-E. Jørgensen, T.R. Jensen, Characterization of gas–solid reactions using in situ powder X-ray diffraction. *Z. Anorg. Allg. Chem.* **640**(15), 3029–3043 (2014)
41. B.R.S. Hansen, K.T. Møller, M. Paskevicius, A.-C. Dippel, P. Walter, C.J. Webb, C. Pistidda, N. Bergemann, M. Dornheim, T. Klassen, J.-E. Jørgensen, T.R. Jensen, In situ X-ray diffraction environments for high-pressure reactions. *J. Appl. Crystallogr.* **48**(4), 1234–1241 (2015)
42. Y.S. Au, M. Ponthieu, R. van Zwielen, C. Zlotea, F. Cuevas, K.P. de Jong, P.E. de Jongh, Synthesis of Mg<sub>2</sub>Cu nanoparticles on carbon supports with enhanced hydrogen sorption kinetics. *J. Mater. Chem. A* **1**(34), 9983 (2013)
43. M. Norek, T.K. Nielsen, M. Polanski, I. Kuncce, T. Płociński, L.R. Jaroszewicz, Y. Cerenius, T.R. Jensen, J. Bystrzycki, Synthesis and decomposition mechanisms of ternary Mg<sub>2</sub>CoH<sub>5</sub> studied using in situ synchrotron X-ray diffraction. *Int. J. Hydrog. Energy* **36**(17), 10760–10770 (2011)
44. L. Pasquini, E. Callini, M. Brighi, F. Boscherini, A. Montone, T.R. Jensen, C. Maurizio, M.V. Antisari, E. Bonetti, Magnesium nanoparticles with transition metal decoration for hydrogen storage. *J. Nanopart. Res.* **13**(11), 5727–5737 (2011)
45. H. Shao, M. Felderhoff, F. Schüth, Hydrogen storage properties of nanostructured MgH<sub>2</sub>/TiH<sub>2</sub> composite prepared by ball milling under high hydrogen pressure. *Int. J. Hydrog. Energy* **36**(17), 10828–10833 (2011)
46. M. Ponthieu, F. Cuevas, J.F. Fernández, L. Laversenne, F. Porcher, M. Latroche, Structural properties and reversible deuterium loading of MgD<sub>2</sub>–TiD<sub>2</sub> Nanocomposites. *J. Phys. Chem. C* **117**(37), 18851–18862 (2013)
47. E. Callini, L. Pasquini, L.H. Rude, T.K. Nielsen, T.R. Jensen, E. Bonetti, Hydrogen storage and phase transformations in Mg–Pd nanoparticles. *J. Appl. Phys.* **108**(7), 073513 (2010)
48. M. Ponthieu, Y.S. Au, K. Provost, C. Zlotea, E. Leroy, J.F. Fernández, M. Latroche, P.E. de Jongh, F. Cuevas, Nanoconfinement of Mg<sub>6</sub>Pd particles in porous carbon: size effects on structural and hydrogenation properties. *J. Mater. Chem. A* **2**(43), 18444–18453 (2014)
49. M. Polanski, T.K. Nielsen, Y. Cerenius, J. Bystrzycki, T.R. Jensen, Synthesis and decomposition mechanisms of Mg<sub>2</sub>FeH<sub>6</sub> studied by in situ synchrotron X-ray diffraction and high-pressure DSC. *Int. J. Hydrog. Energy* **35**(8), 3578–3582 (2010)
50. M. Polanski, T. Płociński, I. Kuncce, J. Bystrzycki, Dynamic synthesis of ternary Mg<sub>2</sub>FeH<sub>6</sub>. *Int. J. Hydrog. Energy* **35**(3), 1257–1266 (2010)
51. S.S. Raman, D.J. Davidson, J.L. Bobet, O.N. Srivastava, Investigations on the synthesis, structural and microstructural characterizations of Mg-based K<sub>2</sub>PtCl<sub>6</sub> type (Mg<sub>2</sub>FeH<sub>6</sub>) hydrogen storage material prepared by mechanical alloying. *J. Alloys Compd.* **333**(1–2), 282–290 (2002)
52. C. Milanese, A. Girella, G. Bruni, V. Berbenni, P. Cofrancesco, A. Marini, M. Villa, P. Matteazzi, Hydrogen storage in magnesium–metal mixtures: reversibility, kinetic aspects and phase analysis. *J. Alloys Compd.* **465**(1–2), 396–405 (2008)
53. T. Liu, T. Zhang, X. Zhang, X. Li, Synthesis and hydrogen storage properties of ultrafine Mg–Zn particles. *Int. J. Hydrog. Energy* **36**(5), 3515–3520 (2011)
54. S. Deledda, B.C. Hauback, H. Fjellvåg, H-sorption behaviour of mechanically activated Mg–Zn powders. *J. Alloys Compd.* **446–447**, 173–177 (2007)
55. T.A. Webb, C.J. Webb, A.K. Dahle, E.M. Gray, In-situ neutron powder diffraction study of Mg–Zn alloys during hydrogen cycling. *Int. J. Hydrog. Energy* **40**(25), 8106–8109 (2015)
56. D. Shechtman, I. Blech, D. Gratias, J.W. Cahn, Metallic phase with long-range orientational order and no translational symmetry. *Phys. Rev. Lett.* **53**(20), 1951–1953 (1984)
57. W. Steurer, S. Deloudi, Fascinating quasicrystals. *Acta Crystallogr. A* **64**(Pt 1), 1–11 (2008)
58. Z. Luo, S. Zhang, Y. Tang, D. Zhao, Quasicrystals in as-cast Mg–Zn–RE alloys. *Scr. Metall. Mater.* **28**(12), 1513–1518 (1993)
59. A. van Blaaderen, Materials science: quasicrystals from nanocrystals. *Nature* **461**(7266), 892–893 (2009)
60. A.M. Viano, R.M. Stroud, P.C. Gibbons, A.F. McDowell, M.S. Conradi, K.F. Kelton, Hydrogenation of titanium-based quasicrystals. *Phys. Rev. B: Condens. Matter* **51**(17), 12026–12029 (1995)
61. A.M. Viano, E.H. Majzoub, R.M. Stroud, M.J. Kramer, S.T. Mixture, P.C. Gibbons, K.F. Kelton, Hydrogen absorption and storage in quasicrystalline and related Ti–Zr–Ni alloys. *Philos. Mag. A* **78**(1), 131–142 (1998)
62. M. Sahlberg, Y. Andersson, Hydrogen absorption in Mg–Y–Zn ternary compounds. *J. Alloys Compd.* **446–447**, 134–137 (2007)
63. X. Luo, D.M. Grant, G.S. Walker, Hydrogen storage properties for Mg–Zn–Y quasicrystal and ternary alloys. *J. Alloys Compd.* **645**, S23–S26 (2015)

64. R.V. Denys, V.A. Yartys, Effect of magnesium on the crystal structure and thermodynamics of the  $\text{La}_{3-x}\text{Mg}_x\text{Ni}_9$  hydrides. *J. Alloys Compd.* **509**, S540–S548 (2011)
65. R.V. Denys, V.A. Yartys, C.J. Webb, Hydrogen in  $\text{La}_2\text{MgNi}_9\text{D}_{13}$ : the role of magnesium. *Inorg. Chem.* **51**(7), 4231–4238 (2012)
66. V. Yartys, R. Denys, Structure–properties relationship in  $\text{RE}_3 - x\text{Mg}_x\text{Ni}_9\text{H}_{10-13}$  (RE = La, Pr, Nd) hydrides for energy storage. *J. Alloys Compd.* **645**, S412–S418 (2015)
67. R. Denys, V. Yartys, E. Gray, C. Webb,  $\text{LaNi}_5$ -assisted hydrogenation of  $\text{MgNi}_2$  in the hybrid structures of  $\text{La}_{1.09}\text{Mg}_{1.91}\text{Ni}_9\text{D}_{9.5}$  and  $\text{La}_{0.91}\text{Mg}_{2.09}\text{Ni}_9\text{D}_{9.4}$ . *Energies* **8**(4), 3198–3211 (2015)
68. Q. Lai, M. Paskevicius, D.A. Sheppard, C.E. Buckley, A.W. Thornton, M.R. Hill, Q. Gu, J. Mao, Z. Huang, H.K. Liu, Z. Guo, A. Banerjee, S. Chakraborty, R. Ahuja, K.-F. Aguey-Zinsou, Hydrogen storage materials for mobile and stationary applications: current state of the art. *ChemSusChem.* **8**(17), 2789–2825 (2015)
69. D.A. Sheppard, C. Corgnale, B. Hardy, T. Motyka, R. Zidan, M. Paskevicius, C.E. Buckley, Hydriding characteristics of  $\text{NaMgH}_2\text{F}$  with preliminary technical and cost evaluation of magnesium-based metal hydride materials for concentrating solar power thermal storage. *RSC Adv.* **4**(51), 26552–26562 (2014)
70. J.C. Crivello, J. Zhang, M. Latroche, Structural stability of ABy Phases in the (La, Mg)–Ni system obtained by density functional theory calculations. *J. Phys. Chem. C* **115**(51), 25470–25478 (2011)
71. J.-C. Crivello, M. Gupta, M. Latroche, First principles calculations of (La, Mg) $_2\text{Ni}_7$  hydrides. *J. Alloys Compd.* **645**, S5–S8 (2015)
72. V.A. Yartys, V.E. Antonov, A.I. Beskrovnyy, J.C. Crivello, R.V. Denys, V.K. Fedotov, M. Gupta, V.I. Kulakov, M.A. Kuzovnikov, M. Latroche, Y.G. Morozov, S.G. Sheverev, B.P. Tarasov, Hydrogen-assisted phase transition in a trihydride  $\text{MgNi}_2\text{H}_3$  synthesized at high  $\text{H}_2$  pressures: thermodynamics, crystallographic and electronic structures. *Acta Mater.* **82**, 316–327 (2015)
73. D.A. Sheppard, M. Paskevicius, T.D. Humphries, M. Felderhoff, G. Capurso, J. Bellosta von Colbe, M. Dornheim, T. Klassen, P.A. Ward, J.A. Teprovich Jr., C. Corgnale, R. Zidan, D.M. Grant, C.E. Buckley, Metal hydrides for concentrating solar-thermal power energy storage. *J. Appl. Phys. A* (in preparation)
74. J.-C. Crivello, B. Dam, R.V. Denys, M. Dornheim, D.M. Grant, J. Huot, T.R. Jensen, P. de Jongh, M. Latroche, C. Milanese, D. Milčius, G.S. Walker, C.J. Webb, C. Zlotea, V.A. Yartys, Review of magnesium hydride based materials: development and optimisation. *Appl. Phys. A*. doi:10.1007/s00339-016-9602-0
75. P. de Rango, P. Marty, D. Fruchart, Integrated with FC H storage systems utilising magnesium hydride: experimental studies and modelling. *Appl. Phys. A* (in preparation)